~~COO-3158-82~~
DOE/ER/03158-82

SINGLE ATOM SPUTTERING EVENTS: DIRECT OBSERVATION OF NEAR-SURFACE DEPLETED ZONES IN ION-IRRADIATED TUNGSTEN

by

Michael I. Current, Ching-Yeu Wei and David N. Seidman

March 1980

Report #4193

Issued by

The Materials Science Center

Prepared for

THE U.S. DEPARTMENT OF ENERGY UNDER CONTRACT NO. DE-AS02-76ER03158.

DISCLAIMER

SINGLE ATOM SPUTTERING EVENTS: DIRECT OBSERVATION OF NEAR-SURFACE DEPLETED ZONES IN ION-IRRADIATED TUNGSTEN†

by

Michael I. Current, Ching-Yeu Wei* and David N. Seidman

Cornell University, Department of Materials Science and Engineering
and the Materials Science Center, Bard Hall, Ithaca, New York 14853 USA

ABSTRACT

The three-dimensional spatial arrangement of vacancies contained in depleted zones (DZs), of ion-irradiated tungsten specimens, was determined with atomic resolution by the field-ion microscope (FIM) technique. These DZs were detected in the near-surface region of specimens which had been irradiated *in situ* at $\leq$15 K with 20 keV W^+, 30 keV W^+, Kr^+, Cu^+ or Ar^+ ions. The values of the ion dose employed were small ($\leq 10^{13}$ ions cm^{-2}); therefore, each DZ analyzed was the result of the impact of a single projectile ion. At the irradiation temperature ($\leq$15 K) both the self-interstitial atoms and vacancies were immobile, so that the primary state of radiation damage was preserved. The following properties of each DZ were determined: (1) the total number of vacancies; (2) the number of vacancies in the near-surface region; (3) the spatial extent--that is, the dimensions required to determine a volume; (4) the average vacancy concentration; (5) the average vacancy concentration associated with the near-surface region; (6) the first-nearest neighbor cluster distribution for the vacancies in the near-surface region; (7) the radial distribution function of all the vacancies; (8) the distribution of vacancies as a function of depth normal to the irradiated surface; and (9) the sputtering yield. Most of the above properties of the near-surface DZs had similar values to those of the DZs detected in the bulk of the FIM specimens. The total number of vacancies detected in the near-surface region was approximately consistent with theoretical estimates of the average sputtering yield. The sputtering yield of individual DZs exhibited significant fluctuations from the measured average sputtering yield.

---

† This research was supported by the U.S. Department of Energy under Contract No. DE-AS02-76ER0315. Additional support was received from the National Science Foundation through the use of the technical facilities of the Materials Science Center at Cornell University.

* Now at the General Electric Corporate Research and Development Laboratory, Schenectady, New York 12305 USA

§ 1. INTRODUCTION

The study of sputtering--the erosion of solid surfaces as a result of energetic particle bombardment--has produced a voluminous experimental and theoretical literature over the past decade; for reviews, see Carter and Colligon (1968), Sigmund (1972), Andersen (1974), McCracken (1975) and Thompson (1978). The bulk of the experimental studies can be roughly divided into the following two broad categories: (1) the measurement of the amount, energy and direction of ejection of the target material as a function of the mass, energy and direction of impingement of the incident ions or atoms (Thompson 1978); and (2) microscopic observations of the changes in the topology of the surface caused by the sputtering processes (for examples, see Hermanne 1973 and Whitton et al. 1978). The typical microscopic observations of sputtered surfaces were for specimens which had been irradiated to high doses (10^{15}-10^{19} ions cm^{-2}) and were made with modest spatial resolution ($\sim$100 - 10,000 Å). There have also been several attempts to utilize the atomic resolution of the field-ion microscope (FIM) to study radiation damage, produced by low-energy ions, in the surfaces of tungsten specimens (Gregov and Lawson 1972 and Walls et al. 1976).

We recently employed the FIM technique to study the sputtering of clean tungsten surfaces by 30 keV Cu^+ ions (Current and Seidman 1980). And in this paper we have presented the results of a systematic and quantitative FIM study of the vacancy structure of displacement cascades--hereinafter called depleted zones (DZs)--which were produced in the near-surface region of tungsten specimens by 20 keV W^+, 30 keV W^+, Kr^+, Cu^+ or Ar^+ ions. The character of DZs in the near-surface region--defined precisely in §3--was essential to understanding sputtering on an atomic scale. The temperature of the specimen was maintained at $\leq$15 K throughout the course of the in situ irradiation and subsequent examination of the specimen by pulse field evaporation. For a specimen temperature of $\leq$15 K, in the case of ion-irradiated tungsten, both vacancies and self-interstitial atoms (SIAs) were found to be immobile (Scanlan, Styris and Seidman 1971a and 1971b and Seidman 1978). Thus our experimental conditions preserved the primary state of radiation damage; that is, the three-dimensional spatial arrangement of point

defects, after all the initial energy of the projectile ions had been dissipated and in the complete absence of any long range migration of the point defects produced by the irradiation. The values of the doses employed for the irradiations were small enough so that each DZ detected was associated with the impact of a single projectile ion; therefore, there was no overlap of the DZs.

The DZs that contained a portion of their volume in the near-surface region were analyzed completely--with atomic resolution--and their principal properties were compared with those DZs found in the bulk of the FIM specimens (Wei 1978, Wei and Seidman 1979 and Current, Wei and Seidman 1980). Their principal properties were found to be very similar to these same properties for the DZs found in the bulk of the specimens. Radiation damage theory was used to calculate values of these features and, in general, reasonable agreement was found between the experimental and theoretical values. The total number of vacancies detected in the near-surface region was found to be approximately consistent with estimates of the average value of the theoretical sputtering yield. However, the values of the sputtering yields for individual DZs were as much as seven times greater than the average value of the measured sputtering yield; thus providing direct evidence for the existence of fluctuations in the sputtering yield.

§ 2. EXPERIMENTAL DETAILS

2.1. Specimen Chemistry and Preparation

The FIM specimens were prepared from two-pass zone-refined tungsten rods (Wilson and Seidman 1975) which had been grown so that the specimen axis was parallel to the [111] crystal axis. This particular orientation was chosen because it maximized the number of high-index planes exposed on the surface of an FIM specimen. The zone-refined rods were electropolished to a diameter of $\sim$0.25 mm in a 1N solution of a NaOH at a potential of 4 V (a.c.). Sharply pointed ($\sim$100 Å radius tip) FIM specimens were then prepared from the 0.25 mm diameter rods employing the same 1N NaOH solution. The specimens were then field evaporated to a radius of greater than 250 Å.

2.2. The Irradiation Procedure

A Hill-Nelson (1965) sputtered-metal ion source provided an ion beam of the various projectiles used for the irradiations. The ion beam was analyzed magnetically and directed into an ultra-high vacuum FIM which was attached to the Hill-Nelson ion source via a three-stage differentially pumped flight tube (Scanlan, Sytris and Seidman 1971a). This arrangement allowed for the in situ irradiation, of FIM specimens, at $(5\text{-}10)\times10^{-10}$ torr with a gas pressure of $(2\text{-}5)\times10^{-6}$ torr measured above the diffusion pump which evacuated the ion source. All irradiations were performed in situ with the specimen at <15 K, in the absence of both the imaging electric field and gas. The maintenance of a low background pressure in the FIM during an irradiation was essential to prevent any possible surface corrosion effects due to the adsorption of gases from the background gases in the FIM.† For a typical flux of 2×10^{10} ions cm^{-2} sec^{-1}, a dose of 5×10^{12} ions cm^{-2} was collected in ~5 minutes. Doses in the range 10^{12} to 10^{13} ions cm^{-2} produced from one to five, well separated DZs in the volume of the FIM specimens examined. For the flux and dose values employed the time required to form an adsorbed monolayer was always greater than the irradiation period. Upon the completion of an irradiation the voltage was returned immediately to the best image voltage value to prevent the adsorption of gases from the background pressure.

The temperature of the FIM specimen was monitored, during the course of each experiment, with a miniature platinum resistance thermometer mounted near the tail of the cryostat. For further details regarding the cryostat, temperature measurement, the sputtered-metal ion source and the irradiation facility, see our earlier publications (Seidman et al. 1969, Seidman and Scanlan 1971, Scanlan et al. 1971a, Pétroff and Seidman 1973 and Wilson and Seidman 1975).

---

† Mulson and Müller (1963) observed, by field-ion microscopy, corrosion effects on tungsten surfaces in partial pressures of N_2 and CO. The pressures of the gases used by Mulson and Müller were at least a factor of 10^4 to 10^6 greater than the partial pressure of these same gases in our FIM. At a background pressure of 6×10^{-10} torr the main residual gases in our FIM were hydrogen and CO. For the vacuum conditions we employed there were no observable corrosion effects.

2.3. Data recording system and the analysis of ciné film

The helium FIM images were observed with the aid of an internal image-intensification system based on a Galileo 76 mm diameter channel electron-multiplier array (Brenner and McKinney 1970). The FIM images were recorded on Kodak Plus-X 35 mm negative film with the aid of an Automax ciné camera equipped with a 1000 ft. film chamber.

The examination of the bulk of an irradiated specimen was accomplished by the dissection of each specimen, on an atom-by-atom basis, employing the pulse field evaporation technique (Robertson and Seidman 1968, Seidman 1973, 1976 and 1978). An FIM image was recorded (typically a 1 sec exposure) after a field-evaporation pulse had been applied to the specimen; this pulse had a width of $\sim$5 msec and an amplitude of $\sim$20% of the best image voltage. On the average, each field evaporation pulse removed one to three atoms from a (512) plane. Approximately 1000 feet of film ($\sim 1.6 \times 10^4$ frames) were exposed during the pulse dissection of a single irradiated specimen. The exposed and developed ciné film was analyzed with a Vanguard Motion Analyser which was equipped with x-y crosshairs and a position readout (Scanlan et al. 1969); the motion analyser was interfaced to a Houston Omnigraphic 200 x-y recorder (Wei 1978).

The ciné film was first scanned to locate the general positions of the DZs in the FIM specimen. The DZs were then reconstructed in three dimensions, by analyzing the ciné film on a frame-by-frame basis and locating the positions of all the atoms and vacant lattice sites[†]--hereinafter vacancies--in each low index plane where radiation damage was found (Beavan, Scanlan and Seidman 1971, Wilson and Seidman 1973, Wei 1978, Wei and Seidman 1979 and Current and Seidman 1980). The observed radiation damage was separated into the following two groups: (1) vacancies - they were often found in closely associated clusters (i.e., DZs); and (2) SIAs which were generally found at a distance from the DZs (Beavan, Scanlan and Seidman 1971 and Wei and Seidman 1980). In this paper only the results concerning the vacancy damage were presented.

---

† At the irradiation temperatures (<15 K) we employed the equilibrium concentration of thermally generated vacancies was, of course, totally insignificant.

A network of fiducial marks which had been scratched in the phosphor screen, of the internal image-intensification system, were used to compensate for the slight shifts in the centering of the individual frames of film during the scanning procedure. On the average, 50 frames of film were recorded and analyzed for the pulse dissection of each atomic plane. The complete set of lattice site positions for all the vacancies, in the different (hkl) planes, for each DZ were transformed to a single coordinate system based on the [100], [010] and [001] unit vectors of the body-centered cubic lattice (Wei 1978).

§ 3. THE NEAR-SURFACE REGION

The majority of the experimental and theoretical results on sputtering have been concerned with the atoms that were ejected from the surface of the target, rather than the detailed point defect nature of the resulting radiation damage in the surface. In order to compare our results to this large body of information we made a first-order estimate of the depth, measured from the initial surface of the target, through which tungsten atoms were most likely able to have contributed to the ejected flux of atoms produced by the impact of a single ion on the target. This so-called source depth has been generally--although not universally--believed to have a thickness of the order of a few atomic layers. First, we used Sigmund's (1969a and 1969b) continuum treatment of sputtering and obtained a first order estimate of this source depth of $\sim$6.5 Å for tungsten. A series of molecular dynamic computer simulations of the ejection of copper atoms (Harrison et al. 1978, Winograd et al. 1978 and Garrison et al. 1978 and 1979) from a thin crystallite of copper, produced by the impact of a 600 eV Ar^+ ion on low-index planes, suggested that most of the ejected atoms were located initially within the first two atomic layers (that is, a thickness of a few angstroms). Alternatively, in the microscopic theory of sputtering developed by Thompson (1978) for crystalline materials, an important contribution to the sputtering yield was ascribed to focused collision sequences; this contribution was in addition to the contribution from DZs--collision cascades in Thompson's terminology. In other research on ion-irradiated tungsten

we have actually measured the range of replacement collision sequences (Beavan, Scanlan and Seidman 1971 and Wei and Seidman 1980). Thus, even though the source depth we defined in this paper was less than 3 Å, it was not our intention to exclude the possible role played by focused collision sequences in sputtering.

Figure 1 exhibits: (a) an FIM micrograph of a (433) plane; (b) a drawing of the primitive unit cell (OABC) of the (433) plane and the projection of the atoms that layed within OABC; (c) a photograph of a ball model of the (433) plane. Table 1 lists the coordinates of the atom positions for the first five layers of the (433) plane. The atoms which were actually imaged in a single FIM micrograph (fig. 1a) resided in the topmost (zeroth) layer of the crystal. The atoms in the zeroth layer of the ball model of the (433) plane (fig. 1c) were indicated by dark balls. The hard sphere ball model of the (433) plane (fig. 1c) showed that the atoms in layers 0 to 4 were visible when the (433) plane was viewed along a direction normal to this plane. This crystallographic information was used to define a source depth.

Guided by the results of Harrison and his co-workers the following definition, of the source depth, was used for the high index planes of tungsten examined in this study:

> The near-surface lattice sites were those occupied by hard-sphere atoms whose geometric centers were visible, within the two dimensional primitive unit cell of an (hkl) plane, when viewed along a direction normal to this (hkl) plane in a hard sphere model; that is, along the [hkl] direction for a cubic crystal.

The set of atoms which occupied the near-surface lattice sites defined the near-surface region. The thickness of this near-surface region, as measured from the zeroth layer, was taken to be the source depth; that is, it was assumed to be the origin of the sputtered atoms. It is emphasized that this definition did not exclude the possible contribution of focused collision sequences to the sputtering yield. The vacancies detected in this near-surface region, after an irradiation,

were denoted near-surface vacancies.

Table 2 presents the important parameters used to describe the near-surface region for the principal (hkl) planes used in this study. It should be noted that the thickness of each near surface region listed in Table 2 was less than the lattice constant (a_o) of tungsten (3.165 Å). To examine the atomic details of the three to six planes that were in the near-surface region required extremely careful pulse dissection sequences; thus, for these planes, the average number of frames of film recorded and analyzed was 250 to 300--while for the rest of the specimen the average was 50 frames of film per plane.

§ 4. RESULTS

In this section detailed results were presented on all the DZs that had a portion of their vacancy structure contained within the near-surface region. A total of ten DZs were detected that satisfied this condition. These DZs were produced as the result of in situ irradiations, at <15 K, with 20 or 30 keV W^+, Kr^+, Cu^+ or Ar^+ ions. At a temperature of <15 K we have demonstrated that the SIA in tungsten was completely immobile (Scanlan, Styris and Seidman 1971a and 1971b, Beavan, Scanlan and Seidman 1971, Seidman 1973, Seidman, Wilson and Nielsen 1975a and 1975b, Wei and Seidman 1979). Thus the present experiments examined the primary state of radiation damage in the complete absence of any post-irradiation point-defect long-range migration effects.

Figure 2 exhibits field-ion micrographs of the (222) plane and vicinal planes both before irradiation (fig. 2a) and after field evaporation of two planes following the irradiation with 30 keV Kr^+ ions to a dose of 6×10^{12} ions cm^{-2} at 10 K (fig. 2b). All the radiation damage produced in the (332), (343) and (543) planes was the result of the impact of a single 30 keV Kr^+ ion. Four near-surface vacancies (out of a total of 51 for this DZ) were detected in the third atomic layer of the (332) plane imaged. The radiation damage exhibited in fig. 2b was typical of what we observed in the surface of the specimen immediately after an irradiation. Figure 2c is a schematic diagram of the FIM micrograph shown in fig. 2b.

Figure 3 is a cross-sectional view of the overall primary state of radiation damage in a tungsten specimen which had been irradiated with 30 keV $^{63}Cu^{+}$ ions to a dose of $\approx 7.5 \times 10^{12}$ ions cm^{-2} at ≤ 11 K. The first ~ 50 Å of this specimen was examined employing $\sim 5 \times 10^{3}$ field-evaporation pulses and the remainder of the specimen was examined using an additional $\sim 9.5 \times 10^{3}$ field-evaporation pulses. This figure, in conjunction with fig. 2, illustrates the general ideas behind the pulse dissection experiments.

4.1. The spatial arrangement of the vacancies within the depleted zones.†

First we present pictorial representations of the three-dimensional spatial arrangement of the vacancies contained within all the near-surface region DZs. The OR TEP graphics computer program developed by Johnson (1965, 1970) was used to generate these pictorial representations. The coordinates of the vacancies were used as the input data for the OR TEP program; the direction along which the DZ was viewed was a quantity that could be varied in this computer program. In all the figures of the DZs presented (figs. 4-10) the open and solid circles represented the vacancies, and the length of each connecting bond (i.e., the rod) shown was equal to the first nearest-neighbor distance (2.74 Å) in the tungsten lattice. The solid circles represented those vacancies in each DZ that were in the near-surface region; they were the near-surface vacancies. The tungsten atoms in the perfect lattice surrounding the DZs were omitted for clarity. The pictorial representations of the DZs were exhibited in order of decreasing mass of the projectile ion (M_1).

Figure 4 shows a DZ which was created by the impact of a single 20 keV W^{+} ion. This DZ, denoted DZ0b, was first reported on by Beavan, Scanlan and Seidman (1971). It contained a total of 81 vacancies of which 23 were within the first three (141) planes that comprised the near-surface region.

---

† For the 20 and 30 keV ion irradiations we found a total of 32 DZs. Ten of these DZs had a portion of their volume contained in the near-surface region and the remaining 22 DZs were in the bulk of the FIM specimens. Seven of the ten DZs which had a portion of their volume in the near-surface region were analyzed in complete atomic detail. The properties of these seven DZs constituted the principal results discussed in this paper. Sixteen of the 22 DZs found in the bulk of the specimens were also analyzed completely and their properties provided a reference group for comparison with the properties of the seven near-surface DZs.

Figures 5 and 6 exhibit two different examples of DZs created by the impact of single 30 keV W^+ ions. DZ2c (fig. 5) contained a total of 123 vacancies, of which 45 were in the near-surface region. In the case of DZ2c, the incident ion beam was parallel to the $[\bar{8}\ 11\ 5]$ direction; the ion beam was at an angle of 80° with respect to the normal to the (411) plane. Whereas for DZ3b, the incident ion beam direction ($[\bar{8}\ 11\ 5]$) was at an angle of 85° with respect to the [411] direction; see figs. 5 and 6. It contained a total of 127 vacancies, of which 47 were in the near-surface region.

Figure 7 exhibits DZ14a; it was created by a single 30 keV Kr^+ ion and contained 103 vacancies and 36 near-surface vacancies. The 30 keV Kr^+ ion beam was parallel to the $[\bar{4}13]$ direction, which made an angle of 75° with respect to the [543] direction. The view of DZ14a shown in fig. 7b was obtained by a 40° clockwise rotation about the $[0\bar{1}0]$ direction. Note the orientation of the reference vectors [100], [010] and [001] in the lower left hand corners of figs. 7a and 7b.

Figure 8 shows three different views of DZ7b; it was created as a result of the impact of a single 30 keV Cu^+ ion. The incident ion beam was parallel to the $[\bar{4}31]$ direction, which made an angle of 60° with respect to the normal to the (512) plane. Figure 4a is a view of the DZ along the $[11\bar{3}]$ directions; this direction is almost tangent to the (512) plane. The view in fig. 8b was obtained by a 25° clockwise rotation about the $[0\bar{1}0]$ direction; fig. 8c was obtained by an additional 15° clockwise rotation about this same direction. Figures 8a and 8b illustrate the fact that for 30 keV ion damage in tungsten, where M_1 was significantly less than the mass of the target atom (M_2), there was a general tendency toward the formation of large subclusters (or subcascades) within the DZs (see figs. 8a and 8b). The DZ7b contained 150 vacancies within the first $\sim$25 Å from the same surface. Fifty-one of the total of the 200 vacancies were located in the near-surface region.

Figure 9 exhibits DZ7c which was also created as a result of the impact of a single 30 keV Cu^+ ion. The incident Cu^+ ion beam was parallel to the $[\bar{4}31]$ direction and it made an angle of 80° with respect to the normal to the (433) plane. This DZ contained a total of 144 vacancies of which 54 were in the near-surface region.

Finally, fig. 10 exhibits DZ10a which was created as a result of the impact of a single 30 keV Ar^+ ion. The incident Ar^+ ion beam was parallel to the $[\bar{1}\bar{4}3]$ direction and made an angle of 70° with respect to the normal of the (411) plane. This DZ contained a total of 192 vacancies, of which 70 were in the near-surface region.

4.2. The number of vacancies and the dimensions of the depleted zones

The total number of vacancies (ν) and the number of vacancies within the near-surface region (ν_{ns}), for each DZ, were listed in Table 3. Also listed in this table were the average total vacancy concentration ($\langle c_v \rangle$) and the dimensions of each DZ (λ_1, λ_2 and $\langle\lambda\rangle$).

The volume used to calculate $\langle c_v \rangle$ was an irregularly shaped one. It was calculated employing a series of rectangularly shaped slabs that were normal to the [100] direction--the thickness of each slab corresponded to four (100) interplanar spacings--and the four peripheral surfaces of each slab were constructed to include all the vacancies contained within this volume of the crystal. The quantity $\langle c_v \rangle$ was defined as the total number of vacancies divided by the total number of lattice sites contained in the volume, of the DZ, as defined above. In an effort to take into account the irregular shape of each DZ, the above procedure was repeated for the rectangularly shaped slabs that were normal to the [010] and [001] directions, respectively. Thus the $\langle c_v \rangle$s listed in Table 3 were the average values of these three different determinations.

To determine the dimensions (λ_1, λ_2 and $\langle\lambda\rangle$) of a DZ, the thirteen <100>, <110> and <111>-type directions were employed. For each specific [hkl] direction, the three-dimensional distribution was projected into a plane to produce a two-dimensional distribution; that is, the number of vacancies as a function of distance, in angstroms, for that [hkl] direction. The standard deviations were calculated for each of these 13 different distributions and the largest one was denoted σ_1. The quantity λ_1 was defined to be equal to $2\sigma_1$. The dimension λ_2 was the average value of twice the standard deviations for the distributions which were perpendicular to the direction

associated with λ_1. The average diameter ($<\lambda>$) of a DZ was then defined as†

$$<\lambda>=[\lambda_1(\lambda_2)^2]^{1/3}; \quad (1)$$

and the volume associated with $<\lambda>$ was denoted by V_{dz} and it was given by

$$V_{dz} = \frac{4\pi}{3}\left(\frac{<\lambda>}{2}\right)^3. \quad (2)$$

This volume was approximately 80% greater than the one we used to calculate $<c_v>$. The results presented in Table 3 demonstrated that at constant values of ion energy (E_1) and M_2 the value of $<c_v>$ decreased as M_1 was decreased, and concomitantly the values of λ_1, λ_2 and $<\lambda>$ increased.

4.3. First-nearest neighbor vacancy cluster distributions

The presence of a large number of first-nearest neighbor bonds, in figs. 4 to 10, clearly demonstrated that the vacancies were associated in the form of clusters within the DZs. In this section we considered the first-nearest neighbor distribution of vacancies in the near-surface region. To quantify the vacancy cluster problem we introduced a quantity denoted the fraction of clusters of size n (f_n), which was given by

$$f_n = N_n \Big/ \sum_{j=1}^{n_{max}} N_j, \quad (3)$$

where N_n was the number of first-nearest neighbor vacancy clusters of size n and n_{max} was the size of the largest vacancy cluster. The quantity

$$\sum_{j=1}^{n_{max}} N_j \quad (4)$$

was equal to the total number of first-nearest neighbor vacancy clusters. In fig. 11a we plotted f_n versus n for the near-surface vacancies which were contained in all the

---

† The average radius ($<\lambda>/2$), as defined by eqn. (1), was different from the radius of gyration employed by Sigmund, Scheidler and Roth (1968); in general, we found that $<\lambda>/2$ was approximately equal to one-half of the radius of gyration.

DZs. The best fit line to the data in fig. 11a was given by:

$$f_n \simeq (0.75\pm0.05)n^{-(2.5\pm0.5)}; \qquad (5)$$

this equation was valid between n equal to one to approximately five. For values of $n \gtrsim 5$ there were a few large clusters which produced large fluctuations in the behavior of f_n.

However, it was found possible to represent all the vacancy cluster data by one equation if the quantity f_n was divided by Δn, where Δn was a number which represented an interval in cluster size. The resulting equation was

$$\xi = (f_n/\Delta n) = \left\{ N_n \Big/ \left(\Delta n \sum_{j=1}^{n_{max}} N_j \right) \right\} , \qquad (6)$$

where physically ξ represented the fraction of vacancy clusters of size n in the interval Δn. In fig. 11b we plotted ξ versus n. The values of Δn were selected as follows; for $1 \leq n \leq 5$, $\Delta n=1$; for $6 \leq n \leq 10$, $\Delta n=5$; and for $n>10$, $\Delta n=10$. The best fit line to the data in fig. 11 was given by

$$\xi = (f_n/\Delta n) \simeq (0.75\pm0.05)n^{-(2.5\pm0.5)}; \qquad (7)$$

the slope of this line (-2.5) was found to be insensitive to the choice of Δn. More generally, we discovered that eqn. (7) described the quantity $f_n/\Delta n$ for all the vacancies in all DZs analyzed; for these DZs the value of E_1 ranged from 15 to 70 keV and M_1 was varied between the mass of Ar (39.95 amu) and W (183.85 amu).

In addition to the quantities f_n and ξ, we also employed the quantity F_n, which was given by the expression

$$F_n = N_n/\nu; \qquad (8)$$

physically this quantity represented the fraction of monovacancies (F_1), divacancies (F_2), etc., in each DZ. In fig. 12 we plotted F_1 versus (M_2/M_1). The value of F_1 increased as M_1 was decreased, for <u>all</u> the vacancies contained within the DZs detected that had a portion of their vacancy population in the near-surface region. The range of values found for the bulk DZs also exhibited the same behavior (Wei 1978, Current, Wei and Seidman 1980). Correspondingly, F_1 decreased as M_1 was increased;

that is, a larger fraction of the vacancies were detected in very large first-nearest neighbor clusters for large M_1 (see fig. 11a).

4.4. Radial distribution function

The degree of clustering of the vacancies, on the scale of the order of the dimensions of each DZ, was determined by measuring a specially defined radial distribution function ($\langle N(i) \rangle$). The quantity $\langle N(i) \rangle$ was defined as the average number of vacancies in the i^{th} spherical shell around a vacancy (Wei 1978); this i^{th} spherical shell was enclosed between the spheres of radii r_{i-1} and r_i. The thickness of each shell was set equal to a_o and the number of vacancies in the i^{th} shell was denoted by $B(i,j)$. The quantity $\langle N(i) \rangle$ was then given by

$$\langle N(i) \rangle = \frac{1}{\nu} \sum_{j=1}^{\nu} B(i,j); \qquad (9)$$

where the sum on j extended over all the ν vacancies contained in each DZ.

The quantity $\langle N(i) \rangle$ was plotted as a function of r_i (fig. 13) for the seven near-surface DZs displayed in figs. 4-10. These radial distribution functions exhibited the same trends that the OR TEP pictorial representations indicated (figs. 4-10) but in a more quantitative fashion. For example, the dramatic breakup of DZ7b into two large subclusters (fig. 8) was particularly evident in its radial distribution function (fig. 13e). Also the increase in the average diameter of a DZ with decreasing M_1, at constant E_1, was evident from a comparison of fig. 13b with 13g.

4.5. Radiation damage profiles

The temperature at which each specimen was maintained was below the onset of long-range migration of either the SIA or the vacancy. Thus the position of each vacancy was a direct reflection of the deposited damage energy, for transferred energies greater than the minimum threshold energy of 43 eV (Maury et al. 1978).

Figure 14 exhibits[†]--in histogram form--the fraction of vacancies per 4.5 Å interval, as a function of depth along the normal direction to the irradiated surface for six different DZs; these constitute radiation damage profiles. Also shown

---

† The method of comparing the experimental data with the TRIM calculations, shown in this figure, was suggested by Mr. D. Pramanik.

for comparison are the calculated damage profiles--the smooth solid line--measured in terms of the fraction of the total deposited damage energy (see § 5.2) as a function of depth. These profiles were calculated imploying the Monte Carlo simulation program, TRIM, developed by Haggmark and Biersack (1978); this program employed an amorhpous target and assumed branching binary collisions. In this figure we also indicated: (1) the mean value of the experimental damage profile by, for example, $\langle x \rangle_D$ (DZ2c: W^+ ion); and (2) the mean value of the calculated damage profile by, for example, $\langle x \rangle_D$ (TRIM: 10^3 W^+ ions, 80° incidence). The damage profiles were calculated as a function of depth along the normal to the particular (hkl) plane of interest, with the ion beam parallel to the experimentally determined irradiation direction.

§5. DISCUSSION

§5.1. The spatial arrangement of the vacancies within the depleted zones

Figures 4-10 exhibited atomic resolution images of the spatial distribution of vacancies contained within DZs, which were created as the result of the impact of a single energetic ion† with a tungsten specimen. These DZs had not collapsed into a lower energy configuration--for example, a dislocation loop--despite their high local vacancy concentration (~2 to 15 at.%). Thus the tungsten atoms which remained inside each DZ formed an unambiguous, although somewhat distorted, b.c.c. crystal structure. This high stability of the DZs to collapse allowed the full utilization of the atomic resolution of the FIM technique. In the case of ion-irradiated tungsten the so-called yield factor (Y), determined by transmission electron microscopy (number of visible defect clusters created per incident ion), was always significantly less than unity for E_1 equal to 30 keV (Seidman 1976); the value of Y for tungsten has been determined to be less than 0.1 (Buswell 1970 and Häusserman 1972). Therefore, these studies complemented the transmission electron microscope studies of ion damage in metals (e.g., see Eyre 1973, Wilkens 1975, Merkle 1976, Jenkins and Wilkens 1976, Ruault, Bernas and Chaumont 1979) as we observed that portion of the radiation damage which

---

† Employing the same geometric argument as the one used previously (Beavan et al. 1971, Wilson and Seidman 1973, Wei and Seidman 1978) it was estimated that the maximum number of ion hits on the cross-sectional area of each DZ was always less than one. This value was an upper bound because it neglected the straggling in the range of the incident ions.

was not visible by means of the transmission electron microscope technique.

A visual examination of figs. 4-10 showed that the DZs had the following important physical properties: (1) as M_1 decreased, at constant E_1, the average diameter and therefore the volume of the DZ increased--compare fig. 5 (30 keV W^+ ion) with fig. 10 (30 keV Ar^+ ion); (2) the vacancy concentration within the volume of the DZ was highly non-uniform--e.g., see fig. 8 (30 keV Cu^+ ion); (3) the value of $\langle c_v \rangle$ decreased as M_1 decreased; (4) the tendency toward subcluster formation increased as M_1 decreased; (4) the fraction of vacancies in the near-surface region of each DZ was approximately constant; and (5) the fraction of vacancies that existed as monovacancies increased as M_1 decreased. The analyses we performed were largely aimed at the quantification of the qualitative observations.

5.2. The number of vacancies and the dimensions of the depleted zones

In this section we compared the measured quantities ν and $\langle\lambda\rangle$ (see §4.2) with: (1) experimental values of these quantities for a larger set of DZs (16) which were created in the bulk of the specimens and analyzed by the same techniques; and (2) values of the ν and $\langle\lambda\rangle$ which were <u>calculated</u> employing the assumptions of linear cascade theory and an amorphous solid model (e.g., see Sigmund 1977).

Figure 15 exhibits the quantity ν as function of M_1 for the data listed in Table 2. The dashed lines--labeled "Range of values for bulk DZs"--indicated the full range of the measured values of ν for all DZs created in the bulk of the specimens by 30 keV projectile ions. The values of ν for the DZs detected in the near-surface region were generally within the range of ν values measured for DZs found in the bulk of the specimens.

Since each DZ was created by one incident ion, we obtained an experimental value for the number of Frenkel pairs created by a projectile ion; in our case this number was simply ν--the number of vacancies contained in each DZ. We based our analysis on a modified form of the classical Kinchin-Pease equation (1955) which has been discussed extensively by Robinson and Torrens (1974). The average number of stable Frenkel pairs ($\langle\nu\rangle_{R-T}$) given by the Robinson-Torrens model is:

$$\langle\nu\rangle_{R-T} = \kappa\hat{E}/2E_d, \qquad (10)$$

where κ was the displacement efficiency, $\hat{E}$ the average damage energy and E_d a sharp displacement threshold energy. The original Kinchin-Pease equation is

$$\langle\nu\rangle_{K-P} = E_1/2E_d, \qquad (11)$$

where E_1 was the average energy of the incident projectiles. The quantity E_1 was related to $\hat{E}$ through the expression:

$$\hat{E} = E_1 - \hat{Q}, \qquad (12)$$

where $\hat{Q}$ was the total energy lost from a displacement cascade through all inelastic processes; in the case of metals the inelastic energy transfers did not produce displacements. In the original Kinchin-Pease model, the atoms were considered to be hard spheres and for this case κ was equal to one. The use of more realistic atomic potentials yielded values of κ less than one. For the displacement cascades we studied, low-energy recoil atoms dominated and it was shown both analytically (Sigmund 1969 c) and from computer simulations (Robinson and Torrens 1974, Norgett, Robinson and Torrens 1975) that a value of 0.8 for κ was appropriate for the present experimental situation. For E_d we employed the minimum measured value of 43 eV (Maury et al. 1978). The values of $\hat{Q}$ were calculated employing the tabulations of Winterbon (1975).

The Kinchin-Pease equation predicted a constant value of 349 vacancies; this value was clearly too high (see fig. 15). Equation (10) predicted a value of 218 and 187 vacancies for 30 keV W^+ and Ar^+, respectively; the small but steady decrease in ν with decreasing M_1 was caused solely by the variation in $\hat{Q}$. The calculated value of $\langle\nu\rangle_{R-T}$ can be taken to be $\sim$200, for E_1 = 30 keV, over this range of M_1. The value of $\langle\nu\rangle$ for the DZs in the near-surface region was 148.† And the value of this quantity for the set of 15 DZs found in the bulk created by 30 keV ions was 183±47. The observed spread in ν, at each value of M_1, was mainly the result of the energy straggling of ions along their trajectories in the FIM specimens. It was concluded that: (1) the DZs observed in the near-surface region had approximately

†This number was for the six DZs which were completely analyzed for E_1 = 30 keV.

the same $\langle\nu\rangle$ as the DZs detected at greater depths; (2) and the measured values of $\langle\nu\rangle$ were described reasonably well by the Robinson-Torrens version [eqn. (10)] of the Kinchin-Pease equation; and (3) the good agreement between our $\langle\nu\rangle$ and $\langle\nu\rangle_{R-T}$ implied that the SIAs and the vacancies in the DZs were well separated from one another during the primary displacement events.† Experimental results substantiating point (3) have been recently obtained (Wei and Seidman 1980).

Figure 16a is a plot of the quantity $\langle\lambda\rangle$ (§4.2) versus the Linhard, Scharff and Schiøtt (1963) reduced energy parameter (ε); the experimental data are listed in Table 2. The values of ε were calculated from the expression

$$\varepsilon = \frac{M_2 E_1}{(M_1+M_2)} \Bigg/ \frac{Z_1 Z_2 e^2}{a_{T-F}}, \qquad (13)$$

where Z_1 and Z_2 were the atomic numbers of the projectile and target atoms, respectively, e was the charge on an electron and a_{T-F} was the screening length for a Thomas-Fermi potential (Winterbon 1975). The principal utility of ε was that, for moderately heavy projectile ions in heavy targets, the $\langle\lambda\rangle$s and--to a reasonable approximation--the $\langle c_v\rangle$s of the DZs scaled for all combinations of M_1 and E_1. We used the 16 DZs created by 20 or 30 keV ions and found in the bulk for comparison with the seven DZs found in the near-surface region. The range of $\langle\lambda\rangle$ values measured for the DZs which were found in the bulk of the specimens was indicated by the dashed lines labeled range of values for bulk DZs. The values of $\langle\lambda\rangle$ for the DZs, detected in the near-surface region, were found to lie within this range. One theoretical measure‡ of the "expected" diameter ($\langle D_\delta\rangle$) of a DZ was given as

$$\langle D_\delta\rangle = 2[(\delta\langle\Delta x^2\rangle_D)^{\frac{1}{2}}\delta\langle y^2\rangle_D]^{1/3}, \qquad (14)$$

---

† The experimental data on tungsten did not support Lucasson's (1975) suggestion that an average threshold energy of 110 eV should be used for E_d and that a multiplicative factor of 0.23 should be substituted for $\kappa/2$. The line in fig. 15 denoted $\langle\nu\rangle_L$ represents Lucasson's expression; it was clear that $\langle\nu\rangle_L$ did not represent our data.

‡ Note this definition was consistent with the definition of $\langle\lambda\rangle$ in eqn. (1).

where $(\langle \Delta x^2 \rangle_D)^{\frac{1}{2}}$ and $(\langle y^2 \rangle_D)^{\frac{1}{2}}$ were the second moments of the average elastically-deposited-energy distribution measured parallel and perpendicular, respectively, to the direction of the incident ion-beam; δ was a contraction factor to take account of the smaller volume occupied by the elastic-energy distribution produced by a single ion (Sigmund, Scheidler and Roth 1968, Westmoreland and Sigmund 1970). Figure 16a demonstrated that the measured values of $\langle \lambda \rangle$, in this ε range, were consistently smaller than the $\langle D_\delta \rangle$ values. Since the FIM determinations represented a fairly direct measure of the elastically-deposited-energy distribution, for transferred energies greater than E_d, fig. 16a indicated that the quantity $\langle D_\delta \rangle$ was an upper bound to the average $\langle \lambda \rangle$ of a DZ created by a single ion.

Figure 16b is a graph of the quantity $\langle c_v \rangle$ versus ε. The values of $\langle c_v \rangle$ for the seven DZs detected in the near-surface region and analyzed in complete detail (see Table 3) are plotted on this graph. The error bars for these values of $\langle c_v \rangle$ reflected the variation in the measurement of the volume of a DZ and hence the absolute vacancy concentration.† The dashed lines indicated the range of measured $\langle c_v \rangle$s for the set of DZs found in the bulk of the specimens. This graph demonstrated that all the DZs detected in the near-surface region had values of $\langle c_v \rangle$ which were similar to the values measured for the DZs detected in the bulk of the specimens. We defined the theoretical average vacancy concentration (c_v^*) in a DZ to be given by

$$c_v^* = 0.30 \langle \nu \rangle_{R-T} \Omega_o \Big/ \left[\frac{4\pi}{3} \left(\frac{\langle D_\delta \rangle}{2} \right)^3 \right] , \qquad (15)$$

where Ω_o was the atomic volume and the factor 0.30 accounted for the presence of vacancies outside the ellipsoid of average radius $\langle D_\delta \rangle / 2$. Figure 16b demonstrated that the values of c_v^* were within the range of values measured for the bulk DZs.

5.3. Concentration of near-surface vacancies

The concentration of near-surface vacancies ($\langle c_v \rangle_{ns}$) contained in DZs was taken to be the ratio of ν_{ns} (see Table 3) to the total number of atomic sites contained

---

† The quantity $\langle c_v \rangle$ was calculated from the volume which was described in detail in §4.2 and not the volume based on eqn. (2).

in the (hkl) planes used in the analysis of the near-surface portion of the DZs; the number of these sites varied between ≈ 150 for DZ0b (20 keV W^+) and ≈650 for DZ10a (30 keV Ar^+). The variation of $\langle c_v \rangle_{ns}$ with ε is shown in fig. 17; the dashed curves in this figure indicated the full range of the measured average values of $\langle c_v \rangle$ for all the DZs created in the bulk of the specimens. The values of $\langle c_v \rangle_{ns}$ were generally within the range of values of $\langle c_v \rangle$ for the bulk DZs.

The smaller values of the coordination numbers for the atoms in the near-surface region could have led to a higher value of $\langle c_v \rangle_{ns}$--compared to $\langle c_v \rangle$--if the minimum E_d for this region was significantly less than the E_d for the bulk. Fox example, a reduction of E_d from 43 eV to the sublimation energy (8.7 eV) would have produced a nearly five-fold increase in the value of $\langle c_v \rangle_{ns}$. Such a large influence of the coordination numbers on the production of point defects in the near-surface region was not observed in our studies.

5.4. First-nearest neighbor vacancy cluster distributions†

Figure 11 demonstrated that it was possible to describe the distribution of the first-nearest neighbor vacancy clusters by a single equation. In addition, the same functional dependence [eqn. (7)] was found to hold for: (1) the near-surface vacancies in a single DZ (Current and Seidman 1980); (2) all the vacancies contained with a single DZ (Current and Seidman 1980); and (3) all the vacancies contained within DZs which had been created by the impact of single ions with M_1 ranging from 39.95 (Ar) to 183.85 (W) amu and E_1 ranging from 15 to 70 keV (Current, Wei and Seidman 1980). The fact that the cluster distribution functions for the vacancies contained within the near-surface region and the bulk of the specimens were essentially the same indicated that the process of vacancy formation was <u>not</u> significantly altered for the near-surface vacancies by the presence of the surface. This was in agreement with the discussion presented in §5.3.

The general trend that F_1 increased as M_2/M_1 increased--that is, with decreasing M_1 --for all the vacancies contained within the DZs--was a physically reasonable re-

† A possible relationship between the first-nearest neighbor vacancy cluster distributions and the sputtering of multiation clusters (multimers) was discussed in the Appendix.

sult; since it was expected that the value of $\langle\lambda\rangle$ would increase as M_1 was decreased and the value of ν would remain approximately constant--at a constant E_1 of 30 keV--for the range of M_1 studied. These two results implied that the mean spacing between any two displacement events, which led to permanent vacancies, increased as M_1 was decreased; thus, it was anticipated that the value of F_1 would increase with decreasing M_1. It is expected that with a further decrease in M_1--at constant damage energy $(E_1-\hat{Q})$--the value of F_1 would continue to increase.

5.5. Radial distribution function [$\langle N(i)\rangle$]

The graphs of $\langle N(i)\rangle$ versus r_i, shown in fig. 13, exhibited two major trends as M_1 was decreased from 183.85 (W) to 39.95 (Ar) amu. These trends were: (1) the spatial extent of the DZs increased; and (2) there was a tendency for the DZs to break up into sub-clusters--this effect was clearly seen in fig. 13(e) (also see fig. 8). Sigmund, Scheidler and Roth (1968) predicted that for $M_1 \ll M_2$ there should be subcluster formation--subcascades in their vernacular. The tendency to form large subclusters, for $M_1 \ll M_2$, was also observed for the DZs detected in the bulk of the tungsten FIM specimens; for example, see fig. 1 in the paper by Wei and Seidman (1979). The two major trends observed were a result of: (1) an increase in the total path length and projected range of the projectile ion with decreasing M_1; and (2) an increase in the mean free path of the projectile ion--with decreasing M_1--between collisions that involved large energy transfers.

5.6. Radiation damage profiles

Each experimental radiation damage profile exhibited in fig. 14 represented the distribution of vacancies contained within a single DZ. Even for this limited number of vacancies it was clear that the experimental values of $\langle x\rangle_D$ were reasonably close to $\langle x\rangle_D$ (TRIM). The procedure of plotting the fraction of vacancies per specified depth interval versus depth for all the vacancies in a single DZ constituted the first step in the construction of a radiation damage profile with atomic resolution. This procedure applied to a larger number of DZs yielded beautiful radiation damage profiles (Current, Wei and Seidman 1980) in agreement with the calculation of damage distributions.

It has recently been realized that the depth resolution of analytical techniques that involved sputter depth-profiling of alloys was limited by the effects of the disorder and enhanced diffusion created by the impact of the ion beam on the sample (Webb, Carter and Collins 1978, Liau, Tsaur and Mayer 1979 and Rhen, Danyluck and Wiedersich 1979). The results presented in fig. 14 demonstrated that the radiation damage produced by a single ion extended, from the surface, to a depth comparable to $\langle x \rangle_D$ (TRIM). In the régime of high point defect concentration it is expected--at elevated temperatures--that the diffusion rate of the atoms constituting an alloy will be enhanced. Thus each DZ--produced by a single ion in the sputtering process--can result in so-called atomic mixing due to displacement events and the transport of matter due to enhanced diffusion effects.

5.7. Sputtering

It was pointed out in §3 that it is generally, although not universally, believed that the source depth--for the majority of sputtered atoms--has a thickness of the order of a few atomic layers. This result was obtained from several different models of the sputtering process: that is; (1) an analytical model of the elastically deposited energy distribution (Sigmund 1969 a and 1969 b; (2) Monte Carlo calculations of the trajectories of recoil atoms (Shimuzu 1977 and Haggmark and Wilson 1978); and (3) computer-based molecular dynamic models (Harrison et al. 1978, Winograd et al. 1978 and Garrison et al. 1978). We defined a source depth consistent with the above result, which allowed us to determine values of ν_{ns}, for each DZ that had a portion of its vacancy population in the near-surface region; see §3 and Table 1. In the present section we discussed the relationship of ν_{ns} to values of the theoretical sputtering yield $[S_{th}(\theta)]$ and demonstrated that our observations provided direct evidence for the existence of fluctuations in the measured sputtering yield.

We defined a yield of vacancies found in the near-surface region as,

$$S_v = \frac{\text{total number of observed near-surface vacancies}}{\text{total number of DZs detected in the FIM specimens}} = \frac{\sum \nu_{ns}}{\text{total number of ion hits.}} \qquad (16)$$

It was assumed that the total number of DZs detected in the specimens was equal to the total number of ion hits. The total number of DZs included those DZs which were found in poorly resolved planes and were not analyzed in atomic detail. The measured values of $\Sigma\nu_{ns}$, the total number of DZs and S_v are listed in Table 4 for the 20 and 30 keV W^+ and, 30 keV Kr^+ and Cu^+ ion irradiations. The results for the 30 keV Ar^+ irradiations were not included since only a limited volume of the FIM specimen was examined and S_v could not be determined to the same degree of accuracy as in the other cases. The values of S_v for the 30 keV irradiations were all $\sim$18 near-surface vacancies per ion.

The calculated values of $S_{th}(\theta)$ are also listed in table 4. The calculations were based on the amorphous target model of Sigmund (1969a and 1969b) for the case of angle of incidence, $\theta = 60°$, so that

$$S_{th}(60°) \cong S_{th}(0°)/\cos 60° = 2\, S_{th}(0°)$$

and a surface binding energy equal to the sublimation energy for tungsten (8.7 eV).† The values of $S_{th}(60°)$--for the 30 keV ions--varied from 14 to 19 atoms per ion. The approximate agreement between these values and the measured S_v values was taken as evidence that, indeed, the majority of the sputtered atoms produced by the impact of a single ion came from atomic sites in the near-surface region. These results did <u>not</u> exclude the possibility of a contribution to the sputtering yield from focussed collision sequences.

The observation of sputtering effects on an atomic scale--as is possible with the FIM technique--yielded information about statistical fluctuations between individual sputtering events as well as average effects. It was suggested some time ago that the theoretical sputtering yield for a single ion can differ substantially from the average value of the theoretical sputtering yield (Sigmund 1969 a and 1969 b). Westmoreland and Sigmund (1970) estimated that the number of sputtered atoms produced

---

† The quantity $S_{th}(\theta)$ was evaluated for $\theta=60°$ to approximately take into account the large angles of incidence of the ion beam (see §4.1). The question of the proper value of the surface binding energy to use in the calculation of the theoretical sputtering yield can result in a 50% uncertainty in the predicted value of this quantity (Haggmark and Wilson 1978). In view of this problem we have simply employed the sublimation energy.

by a single ion can vary by at least a factor of ten from one ion to the next; they also showed that the ejection of twice the average number of sputtered atoms per ion was not uncommon. The molecular dynamic calculations of Harrison et al. (1978) for the impact of 600 eV Ar^+ ions on the (111) plane of copper also exhibited large fluctuations in the sputtering yield. For example, the impact of some Ar^+ ions produced no ejected atoms while others produced as many as 13 copper atoms; the average calculated sputtering yield was six atoms per ion for the (111) plane.

The fraction of DZs which contained ν_{ns} near-surface vacancies is shown in fig. 18 as a function of ν_{ns}. Note that over 60% of the DZs detected in the FIM specimens contained no near-surface vacancies and--by implication--produced no sputtered atoms. However, those DZs which did contain near-surface vacancies contained a typical value of 45 near-surface vacancies per ion; this value was $\sim$2.5 times greater than the average value of S_v of 17.7. For DZ10a (30 keV Ar^+) the value of S_v was seven times greater than this average value. These fluctuations in the observed value of S_v represent the first direct measurements which implied fluctuations in the sputtering yield per ion that ranged from zero to approximately three times the average sputtering yield.

§ 6. SUMMARY

1. The three-dimensional spatial arrangement of vacancies contained in depleted zones (DZs) in tungsten was determined by the field-ion microscope (FIM) technique. The DZs were detected in the near-surface region of specimens which had been irradiated in situ at 15 K with 20 keV W^+, 30 keV W^+, Kr^+, Cu^+ or Ar^+ ions. Each analyzed DZ had been produced by a single projectile ion.

2. The values of properties of the DZs found in the near-surface region were similar to the values of these same properties for DZs which were detected in the bulk of the FIM specimens. In addition, the value of these properties were in reasonable agreement with estimates based on radiation damage theory.

3. The total number of vacancies detected in the near-surface region was in approximate agreement with theoretical estimates based on Sigmund's continuum model of the average sputtering yield. The number of vacancies in the near-surface region

of individual DZs ranged from three to seven times the value of the measured average sputtering yield.

ACKNOWLEDGEMENTS

We thank Mr. R. Whitmarsh for continued technical assistance, S. Rumsey for her help with the OR TEP program, Dr. A. Macrander for assistance with the TRIM calculations, Mr. D. Pramanik for useful discussions and Mrs. E. Roebig and Ms. B. Wrona for their careful and steady work on the frame-by-frame analysis of the ciné film.

REFERENCES

Andersen, H.H., 1974, in Physics of Ionized Gases 1974, edited by V. Vujnovic (Univ. Zagreb: Inst. Phys.), p. 361.

Beavan, L.A., Scanlan, R.M., and Seidman, D.N. 1971, Acta metall. 19, 1339.

Brenner, S.S., and McKinney, J.T., 1970, Surface Sci., 23, 88.

Buswell, J.T., 1970, Phil. Mag. 22, 787.

Carter, G., and Colligon, J.S., 1968, Ion Bombardment of Solids, (Amsterdam: Elsevier).

Current, M.I., and Seidman, D.N., 1980, accepted for publication in Nuclear Instruments and Methods.

Current, M.I., Wei, C.-Y., and Seidman, D.N., 1980, Cornell Materials Science Center Report #4235.

Eyre, B.L., 1973, J. Phys. F, 3, 422.

Garrison, B.J., Winograd, N. and Harrison, D.E., 1978, J. Chem. Phys., 69, 1440; 1979, J. Vac. Sci. Technol., 16, 789.

Gregov, B., and Lawson, R.P.W., 1972, Can. J. Phys., 50, 791.

Häussermann, F., 1972, Phil. Mag. 25, 583.

Haggmark, L.G., and Biersack, J.P., 1978, Report of the Hahn-Meitner Institut, Berlin 39, W. Germany.

Haggmark, L.G., and Wilson, W.D., 1978, J. of Nuclear Materials, 76-77, 149.

Harrison, D.E., Kelly, P.W., Garrison, B.J., and Winograd, N., 1978, Surface Sci. 76, 311.

Hermanne, N., 1973, Radiat. Effects, 19, 161.

Hill, K.J., and Nelson, R.S., Nuclear Instruments and Methods, 1965, 38, 15.

Jenkins, M.L., and Wilkens, M., 1976, Phil. Mag., 34, 1155.

Johnson, C.K., 1965, 1970, Oak Ridge National Laboratory (U.S.A.), Report No. 3794 plus revisions.

Kinchin, G.H., and Pease, R.S., 1955, Rep. Prog. Phys., 18, 1.

Liau, Z.L., Tsaur, B.Y., and Mayer, J.W., 1979, J. Vac. Sci. Technol., 16, 121.

Lindhard, J., Scharff, M., and Schiøtt, H., 1963, Mat.-fys. Medd. Dan. Vid. Selsk., 33, No. 14.

Lucasson, P., 1975, Int. Conf. on Fundamental Aspects of Radiation Damage in Metals, edited by M.T. Robinson and F.W. Young, Jr. (Springfield, Virginia: National Technical Information Service), p. 42.

Maury, F., Biget, M., Vajda, P., Lucasson, A., and Lucasson, P., 1978, Radiat. Effects, 38, 53.

Merkle, K.L., 1976, Radiation Damage in Metals, edited by N.L. Peterson and S.D. Harkness (Metals Park, Ohio: American Society for Metals), p. 58.

McCracken G., 1975, Rep. Prog. Phys., 38, 241.

Mulson, J.F. and Müller, E.W., 1963, J. Chem. Phys., 38, 2615.

Norgett, M.J., Robinson, M.T., and Torrens, I.M., 1975, Nuclear Engineering and Design, 33, 50.

Pétroff, P., and Seidman, D.N., 1973, Acta metall., 21, 323.

Rehn, L.E., Danyluck, S. and Wiedersich, H., 1979, Phys. Rev. Lett. 43, 1764.

Robinson, M.T., and Torrens, I.M., 1974, Phys. Rev. B, 9, 5008.

Robertson, S.H. and Seidman, D.N., 1968, J. of Scientific Instruments, 1, 1244.

Ruault, M.O., Bernas, H., and Chaumont, J., 1979, Phil. Mag. A, 39, 757.

Scanlan, R.M., Styris, D.L., Seidman, D.N., and Ast, D.G., 1969, Cornell Materials Science Center Report No. 1159.

Scanlan, R.M., Styris, D.L., and Seidman, D.N., 1971 a, Phil. Mag. 23, 1439; 1971 b Phil. Mag. 23, 1459.

Seidman, D.N., 1973, J. Phys. F., 3, 393; 1976, Radiation Damage in Metals edited by N.L. Peterson and S.D. Harkness (Metals Park, Ohio: American Society for Metals), p. 28; 1978, Surface Sci., 70, 532.

Seidman, D.N., and Scanlan, R.M., 1971, Phil. Mag., 23, 1429.

Seidman, D.N., Scanlan, R.M., Styris, D.L., and Bohlen, J.W. 1969, J. of Scientific Instruments 2, 473.

Seidman, D.N., Wilson, K.L., and Nielsen, C.H., 1975 a, Phys. Rev. Lett., 35, 1041; 1975 b, Int. Conf. on Fundamental Aspects of Radiation Damage in Metals, edited by M.T. Robinson and F.W. Young, Jr. (Springfield, Virginia: National Technical Information Service), p. 373.

Shimizu, R., 1977, Proc. 7th Intern. Vac. Congr. and 3rd Intern. Conf. Solid Surfaces (Vienna: International Union for Vacuum Science), p. 1417.

Sigmund, P., 1969 a, Phys. Rev., 184, 383; 1969 b, Phys. Rev., 187,768; 1969 c, Appl. Phys. Lett., 14, 114; 1972, Rev. roum. Phys., 17, 823, 969 and 1079; 1977, Inelastic Ion-Surface Collisions, edited by N.H. Tolk, J.C. Tully, W. Heiland and C.W. White (New York: Academic Press), p. 121.

Sigmund, P., Scheidler, G.P., and Roth, G., 1968, Proc. Int. Conf. Solid-State Physics Research with Accelerators, Brookhaven National Lab. Report No. 50083, p. 374.

Staudenmaier, G., 1972, Radiat. Effects, 13, 87; 1973, Radiat. Effects, 18, 181.

Thompson, M.W., 1978, in Physics of Ionized Gases 1978, edited by R.K. Janev (Beograd: Inst. Phys.), p. 284.

Walls, J.M., Boothby, R.M., and Southworth, H.N., 1976, Surface Sci., 61, 419.

Webb, R., Carter, G., and Collins, R., 1978, Radiat. Effects, 39, 129.

Wei, C.-Y., 1978, Ph.D. thesis, Cornell University.

Wei, C.-Y. and Seidman, D.N., 1978, Phil. Mag. A, 37, 257; 1979, Appl. Phys. Lett., 34, 622; 1980, Cornell Materials Science Center Report No. 4088.

Westmoreland, J.E., Sigmund, P., 1970, Radiat. Effects, 6, 187.

Whitton, J., Tanovic, L., and Williams, J.S., 1978, Applications of Surface Science, 1, 408.

Wilkens, M., 1975, Int. Conf. on Fundamental Aspects of Radiation Damage in Metals, edited by M.T. Robinson and F.W. Young, Jr. (Springfield, Virginia: National Technical Information Service), p. 98.

Wilson, K.L. and Seidman, D.N., 1973, Defects and Defect Clusters in B.C.C. Metals and their Alloys, edited by R.J. Arsenault (University of Maryland, Department of Chemical Engineering, p. 216, 1975, Radiat. Effects, 27, 67.

Winograd, N., Harrison, D.E., and Garrison, B.J., 1978, Surface Sci., 78, 467.

Winterbon, K.B., 1975, Ion Implantation Range and Energy Deposition Distributions: Low Incident Energies (New York: IFI/Plenum).

APPENDIX

SPUTTERED ION MULTIMERS AND THE NEAR-SURFACE FIRST-NEAREST NEIGHBOR VACANCY CLUSTER DISTRIBUTIONS

Charged multimers (multi-atom clusters) have been detected during the sputtering of both polycrystalline and single crystal tungsten surfaces, by Staudenmaier (1972 and 1973); the specimens were bombarded, at 250°C, with 150 keV He^+, Ne^+, Ar^+, Cu^+, Kr^+, or Xe^+ projectile ions. Staudenmaier made the following observations: (1) the average energy of a multimer decreased as the size of the multimer increased; (2) multimers containing as many as 12 tungsten atoms were detected for an 150 keV Xe^+ bombardment; and (3) both the yields and the maximum multimer size increased as M_1 was increased at constant E_1. On the basis of his observations Staudenmaier suggested that the multimers were generated by "collision cascades--DZs in our nomenclature--which happened to penetrate through the surface of the target." This problem has been studied theoretically by Winograd et al. 1978 who employed a computer simulation approach, to observe the dynamics of multimer formation for a solid copper target bombarded by 600 eV Ar^+ ions. They detected the formation of dimers and trimers within less than ~ 4 Å (the interaction range) of the bombarded surface; however, the multimers did not form by a direct ejection process. They also found that all the multimers detected originated from a roughly circular region--on the surface-- within an area of $\lesssim 70$ $Å^2$ and that most of the trimers contained at least one pair of atoms that were originally first-nearest neighbors in the bombarded surface.

The implications and relationship of our work to the above experiments and calculations were as follows: (1) the increase we observed in the size of the largest nearest-neighbor vacancy cluster with increasing M_1 at constant E_1, was consistent with Staudenmaier's observation that both the yield and maximum multimer size increased with the value of M_1; and (2) our observation of a significant fraction of first-nearest neighbor vacancy clusters in the near-surface region was relevant to Winograd et al.'s result concerning trimers.

Thus, it was our opinion that the distribution of first-nearest neighbor vacancy clusters in the near-surface region must be related to the distribution of multimers observed in the type of experiments and calculations performed by Staudenmaier and Winograd et al., respectively.

To substantiate the above conjecture we used Staudenmaier's (1972) data (see figs. 2, 3 and 4 of his paper) and plotted it in a form that was similiar to the one we used in fig. 11 (b). That is, we plotted the fraction of clusters of size n per interval Δn, $[I_n/(\Delta n \Sigma I_j)]$, versus cluster size (n). The quantity I_n represented the measured intensity of clusters of size n (in arbitary units)--obtained from Staudenmaier's energy spectra--for different energies of the sputtered clusters (E_{spec}). This data is plotted in Fig. 19 for different values of E_{spec} (15, 30 and 15 to 1250 eV); also incicated on this figure are the three lines $0.75n^{-2}$, $0.75n^{-2.5}$ and $0.75n^{-3}$. The most striking common features of the results shown in figs. 11 (b) and 19 were: (1) the fraction of clusters of size n per interval Δn versus n was independent of M_1; and (2) the fractions of sputtered multimers and near-surface vacancies showed a similar dependence on cluster size ($\sim n^{-(2.5\pm1)}$). In addition the increase in the size of the largest multimer observed by Staudenmaier, with increasing M_1, can be compared with our observation--for the larger set of data which included all the DZs found in the bulk of the specimens--that the size of the largest first-nearest neighbor vacancy cluster size increased with increasing M_1. These comparisons suggested that the formation of stable multimers was closely tied to the ejection of atoms from a small region of the surface--specifically, from a network of first-nearest neighbor atomic sites.

Table 1: Table of atomic positions for the (433) plane of the bcc lattice

Atom	Co-ordinates of Position*								
	Relative to Cubic Axes			Relative to O X Y Z					
				$/\sqrt{2}$	$/\sqrt{17}$	$/\sqrt{34}$			
A	0	-2	2	4	0	0	2.8284	0	0
B	3	-3	-1	2	17	0	1.4142	4.1231	0
1	1	-3	1	4	7	-2	2.8284	1.6977	-0.3430
2	2	-4	0	4	14	-4	2.8284	3.3955	-0.6860
3	0	-2	0	2	4	-6	1.4142	0.9701	-1.0290
4	1	-3	-1	2	11	-8	1.4142	2.6679	-1.3720

* The axes OX and OY are indicated in fig. 1 and OZ is the unit vector normal to the (433) plane. The coordinates were given in terms of the length $a_o/2$, where a_o was the lattice parameter of the standard non-primitive unit cell. The coordinates relative to O X Y Z were given both in exact form and also numerically to four significant figures.

Table 2: Important parameters used to describe the near-surface region

Plane (hkl)	Interplanar Spacing hkl (Å)	Number of layers which were visible in a ball model construction of the (hkl) plane.	Thickness of near-surface region (Å)
(222)	0.912	3	2.74
(332)	0.674	4	2.69
(433)	0.542	5	2.71
(543)	0.447	6	2.68
(411)	0.745	3	2.23
(521)	0.577	5	2.88
(721)	0.430	5	2.15
(631)	0.466	6	2.79
(622)	0.477	6	2.86

TABLE 3: Measured values of the parameters used to characterize each depleted zone.

Energy of projectile ion (E_1) in keV	Ion	Depleted zone (DZ)	Total number of vacancies (ν)	Number of vacancies within the near-surface region (ν_{ns})	Average total vacancy concentration $\langle c_v \rangle$ in atomic %	Largest Diameter of the DZ λ_1 in Å	Diameter perpendicular to the direction of $\lambda_1 - \lambda_2$ in Å	Average Diameter of DZ ($\langle\lambda\rangle$) in Å
20	W^+	0b	81	23	13.9	16	9	11
30	W^+	1c	--	46	----	--	--	---
30	W^+	2c	123	45	9	18	13	15
30	W^+	3b	127	47	4.4	44	16	23
30	Kr^+	14a	103	36	5.3	35	14	19
30	Cu^+	6b	---	24	---	--	--	---
30	Cu^+	7b	200	51	5.5	37	20	25
30	Cu^+	7c	144	54	4.6	26	20	22
30	Ar^+	10a	192	70	1.8	49	33	38
30	Ar^+	10b	---	40	---	--	---	---

TABLE 4: Parameters relevant to the sputtering behavior of tungsten surfaces by 20 or 30 keV metal ions

Energy of projectile ion (E_1) in keV	Ion	Total number of near-surface vacancies ($\Sigma\nu_{ns}$)	Total number of DZs in the specimen (ion hits)	Measured sputtering yield (vacancies per ion) S_v	Theoretical sputtering for an incident angle of $\theta = 60°$ (atoms per ion) $S_{th}(\theta = 60°)$
20	W^+	23	2	11.5	16.2
30	W^+	138†	8	17.2	19
30	Kr^+	36	2	18.0	15.4
30	Cu^+	129†	7	18.4	13.8

† These numbers are the sum of the near-surface vacancies for three DZs; see Table 3 for the the individual values for each DZ.

Figure Captions

Figure 1: (a) An FIM image of the vicinal region around the (222) plane of tungsten; note the ten atoms in the outermost (zeroth) layer of the (433) plane.

(b) The primitive mesh (OACB) of the (433) plane and the projection onto that plane of the atoms which lay in the first four planes underneath the zeroth layer.

(c) A ball model of a (433) plane, built on a (200) plane, showing the five layers of atoms which were visible in this construction. The atoms in the primitive mesh and the set of atoms in the four underlying planes are labeled as in (b). The atoms which were visible in an FIM image are indicated by the dark balls.

Figure 2: (a) An FIM image of a tungsten specimen prior to an irradiation.

(b) An FIM image of the same specimen after an <u>in situ</u> irradiation with 30 keV Kr^+ ions and the pulse field evaporation of two (332) layers. The vacancies visible in the (332) plane were 1.34 Å below the irradiated surface.

(c) A schematic of the FIM image shown in (b) indicating the visible atoms (solid black circles) in the (332) plane as well as the four vacant sites (small open circles) which were located during the full, pulse field evaporation of this (332) plane. These vacant sites were among the near-surface vacancies in DZ14a (fig. 7).

Figure 3: A cross-sectional view of an FIM specimen which had been irradiated with 30 keV Cu^+ ions. Two of the five DZs detected in this specimen had a portion of their volume in the near-surface region; they are displayed in figs. 8 and 9.

Figure 4: An OR TEP isometric view of a DZ created by a single 20 keV W^+ ion. DZ0b contained 81 vacancies of which 23 were in the near-surface region (filled circles).

Figure 5: An OR TEP isometric view of DZ2c which was created by a single 30 keV W^+ ion. DZ2c contained 123 vacancies of which 45 were in the near-surface region (filled circles).

Figure 6: An OR TEP isometric view of DZ3b which was created by a single 30 keV W^+ ion. DZ3b contained 127 vacancies of which 47 were in the near-surface region (filled circles).

Figure 7: (a) An OR TEP isometric view of DZ14a which was created by a single 30 keV Kr^+ ion. DZ14a contained 103 vacancies of which 36 were in the near-surface region (filled circles).

(b) An OR TEP isometric view of DZ14a which was obtained by a 40° clockwise rotation about the $[0\bar{1}0]$ direction of the view in (a). Note the relative orientations of the [100], [010] and [001] directions.

Figure 8: (a) An OR TEP isometric view of DZ7b which was created by a single 30 keV Cu^+ ion. DZ7b contained 200 vacancies of which 51 were in the near-surface region (filled circles).

(b) An OR TEP isometric view of DZ7b which was obtained by a 25° clockwise rotation about the $[0\bar{1}0]$ direction.

(c) An OR TEP isometric view of DZ7b obtained by an additional 15° rotation about the $[0\bar{1}0]$ direction of the view in (b).

Figure 9: An OR TEP isometric view of DZ7c which was created by a single 30 keV Cu^+ ion. DZ7c contained 144 vacancies of which 54 were in the near-surface region (filled circles).

Figure 10: An OR TEP isometric view of DZ10a which was created by a single 30 keV Ar^+ ion. DZ10a contained 192 vacancies of which 70 were in the near-surface region (filled circles).

Figure 11: (a) A plot of the fraction of first nearest-neighbor clusters of size n (f_n) among the near-surface vacancies as a function of cluster size (n) for all the DZs detected which had a portion of their volume in the near-surface region.

(b) The cluster size data shown in (a) displayed as a continuous spectrum ($f_n/\Delta n$) with interval sizes, $\Delta n = 1$ for $n \leq 5$; $\Delta n = 5$ for $6 \leq n \leq 10$; and $\Delta n = 10$ for $n > 10$.

Figure 12: The average value of the fraction of monovacancies for vacancies in the near-surface DZs as a function of the target-to-projectile mass ratio. The range of values of the fraction of monovacancies for the DZs found in the bulk of the specimens is indicated by the dotted lines.

Figure 13: The radial distribution function ($\langle N(i) \rangle$) as a function of the shell radius r_i for the seven near-surface DZs.

Figure 14: (a) to (f), The measured fraction of the total number of vacancies per 4.5 Å interval for six near-surface DZs created by 30 keV ions (histogram) and the calculated fraction of elastically deposited energy (smooth curve) as a function of depth normal to the irradiated surface [x(Å)].

Figure 15: The number of vacancies per DZ (ν) for six near-surface DZs which were created by 30 keV ions as a function of the projectile mass (M_1). The range of values for ν for the DZs found in the bulk of the specimens is indicated by the dotted lines. Also indicated are the theoretical estimates for the average value of ν according to the Kinchin-Pease ($\langle \nu \rangle_{K-P}$), Robinson-Torrens ($\langle \nu \rangle_{R-T}$) and Lucasson ($\langle \nu \rangle_L$) models.

Figure 16: (a) The average DZ diameter ($<\lambda>$) as a function of the Linhard-Scharff-Schiøtt energy (ε) parameter for seven near-surface DZs. Also indicated are the range of values for $<\lambda>$ for the DZs found in the bulk and an estimate of the diameter of a DZ according to the model of Sigmund et al. ($<D_\delta>$).

(b) The average vacancy concentration ($<c_v>$) for seven near-surface DZs as a function of ε. Also indicated are the range of values of $<c_v>$ for the DZs found in the bulk of the specimens and an estimate of the vacancy concentration based on $<\nu>_{R-T}$ and $<D_\delta>$.

Figure 17: Concentration of vacancies in the near-surface region ($<c_v>_{ns}$) for ten near-surface DZs as a function of ε. Also indicated is the range of values for $<c_v>$ for the DZs found in the bulk of the specimens.

Figure 18: The fraction of DZs with ν_{ns} near-surface vacancies as a function of ν_{ns} for all of the DZs created by 30 keV W^+, Kr^+ or Cu^+ ions.

Figure 19: The fraction of stable charged multimers, ejected from tungsten during bombardment by 150 keV ions, as a function of miltimer size n; from the data of Staudenmaier (1972). Shown are the charged multimer fractions for sputtered cluster energies of (1) 15eV, for all ions (●); (2) 30eV, for Xe^+ ions (○); and (3) the average for all energies between 15 to 1250 eV and all ion masses (◇). Compare this figure with fig. 11b.

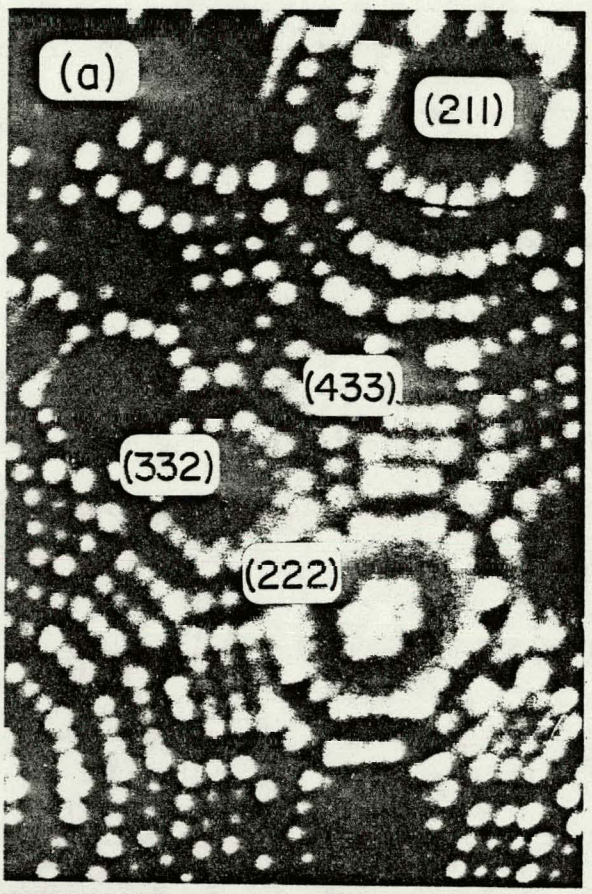

BCC (433)

(b)

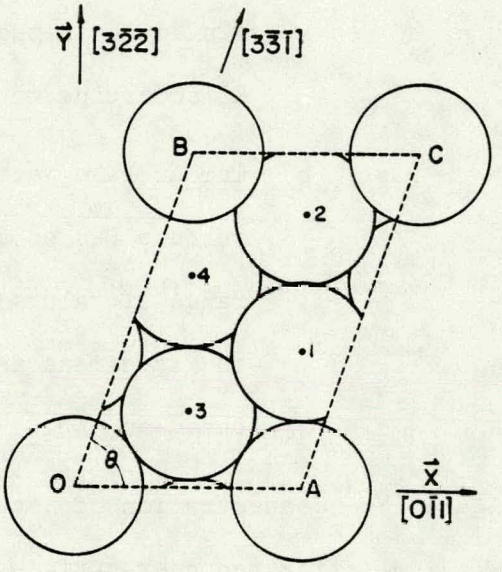

$\theta = 71.07°$

$\vec{u} = \overrightarrow{OA} = a_o[0\bar{1}1]$

$\vec{v} = \overrightarrow{OB} = \frac{a_o}{2}[3\bar{3}\bar{1}]$

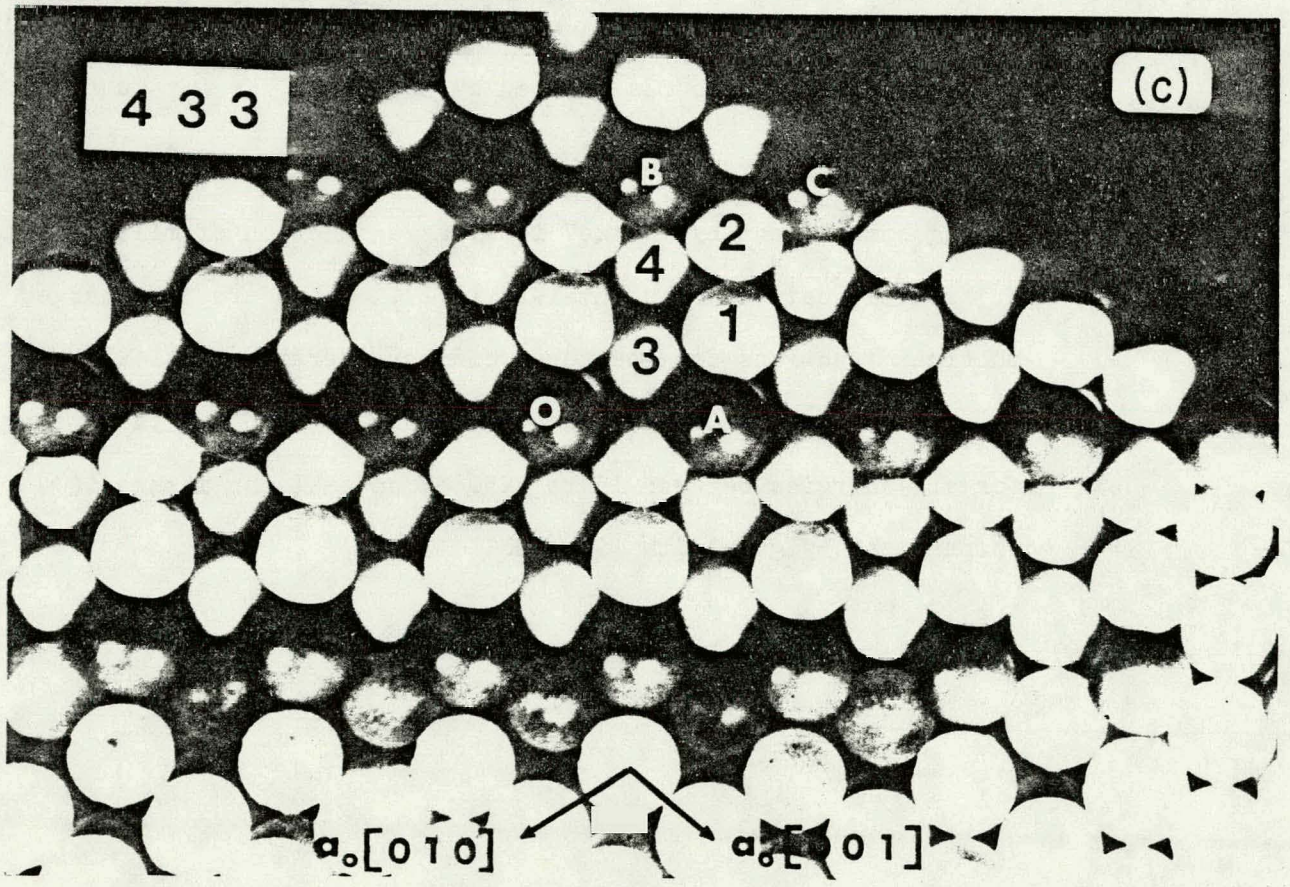

Figure 1

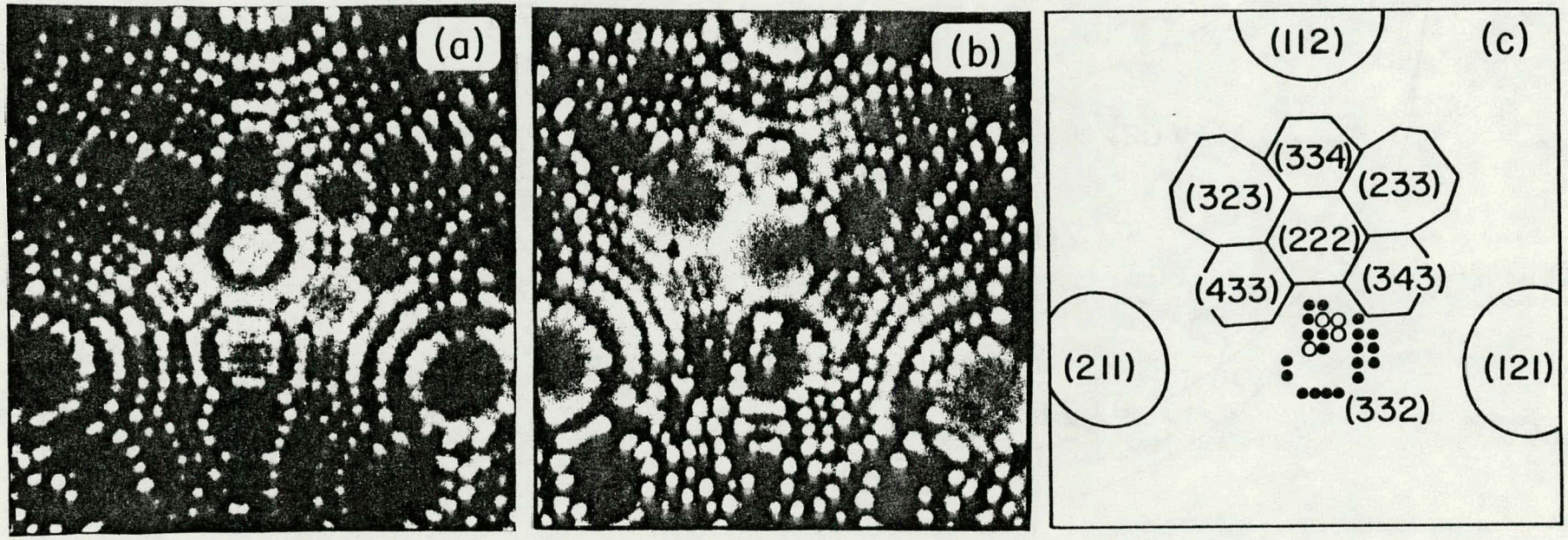

Figure 2

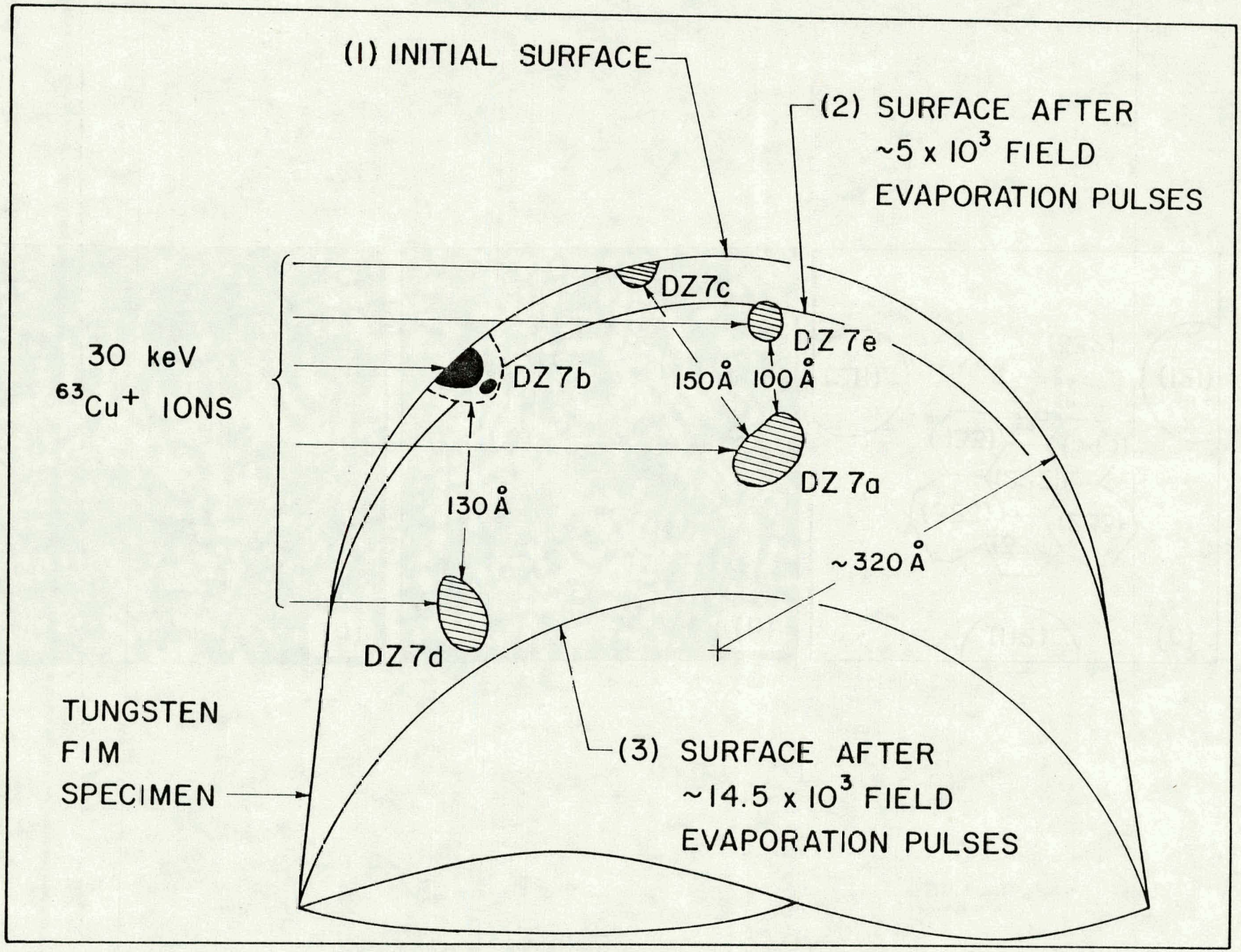
(1) INITIAL SURFACE
(2) SURFACE AFTER
~5 x 10^3 FIELD
EVAPORATION PULSES
30 keV
63Cu+ IONS
DZ7c
DZ7e
DZ7b
150Å
100Å
DZ7a
130Å
~320Å
DZ7d
TUNGSTEN
FIM
SPECIMEN
(3) SURFACE AFTER
~14.5 x 10^3 FIELD
EVAPORATION PULSES

Figure 3

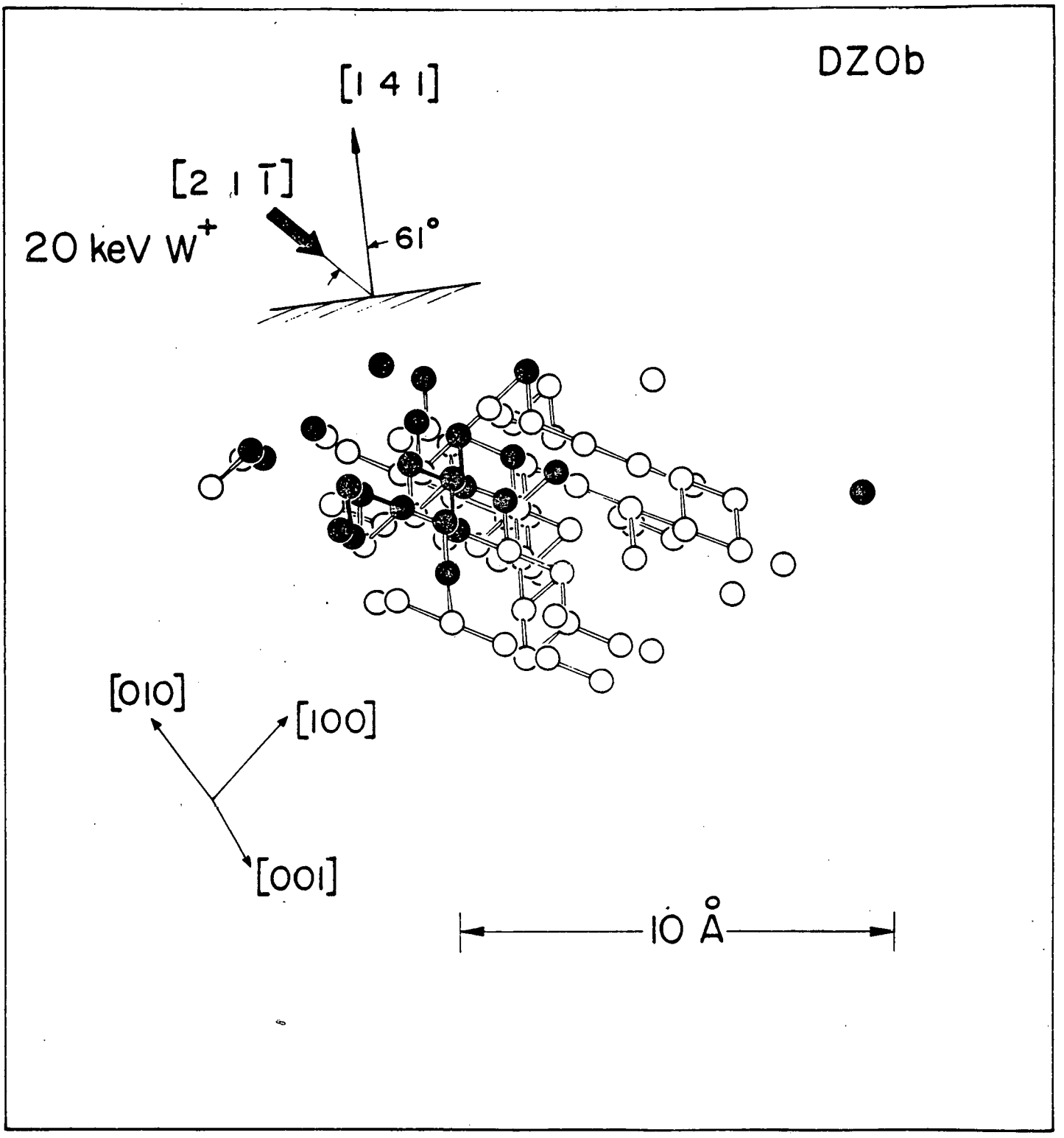

Figure 4

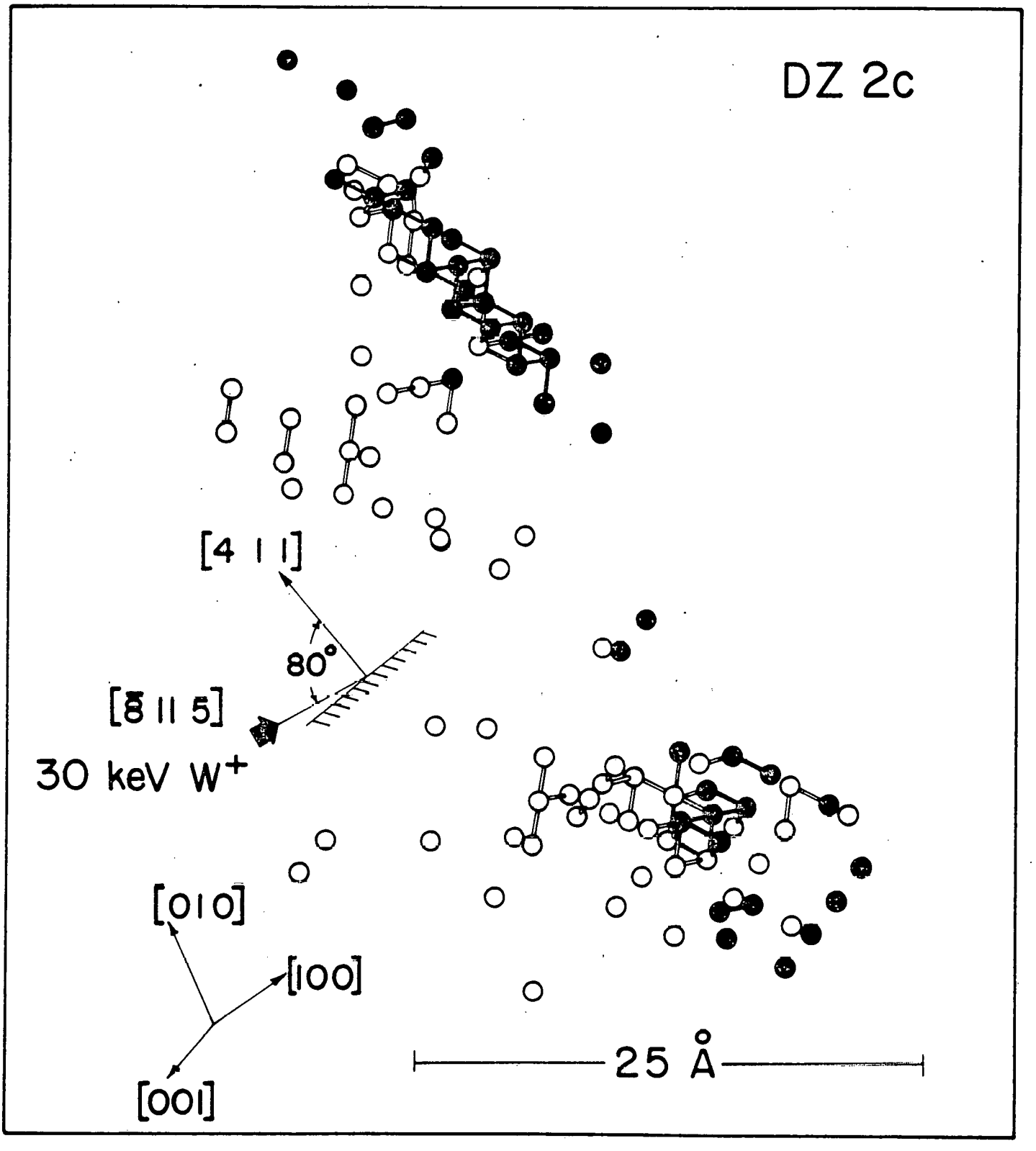

Figure 5

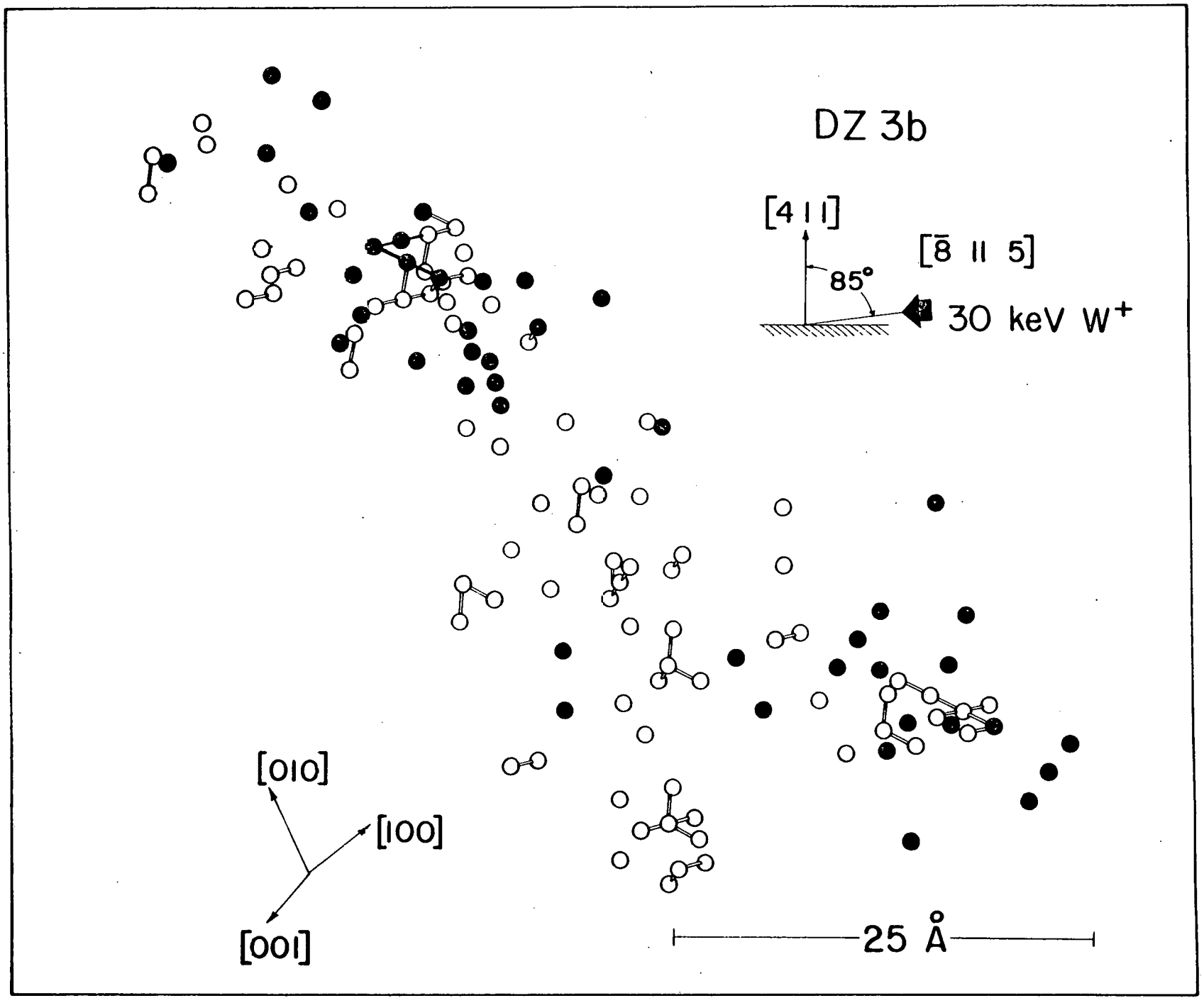

Figure 6

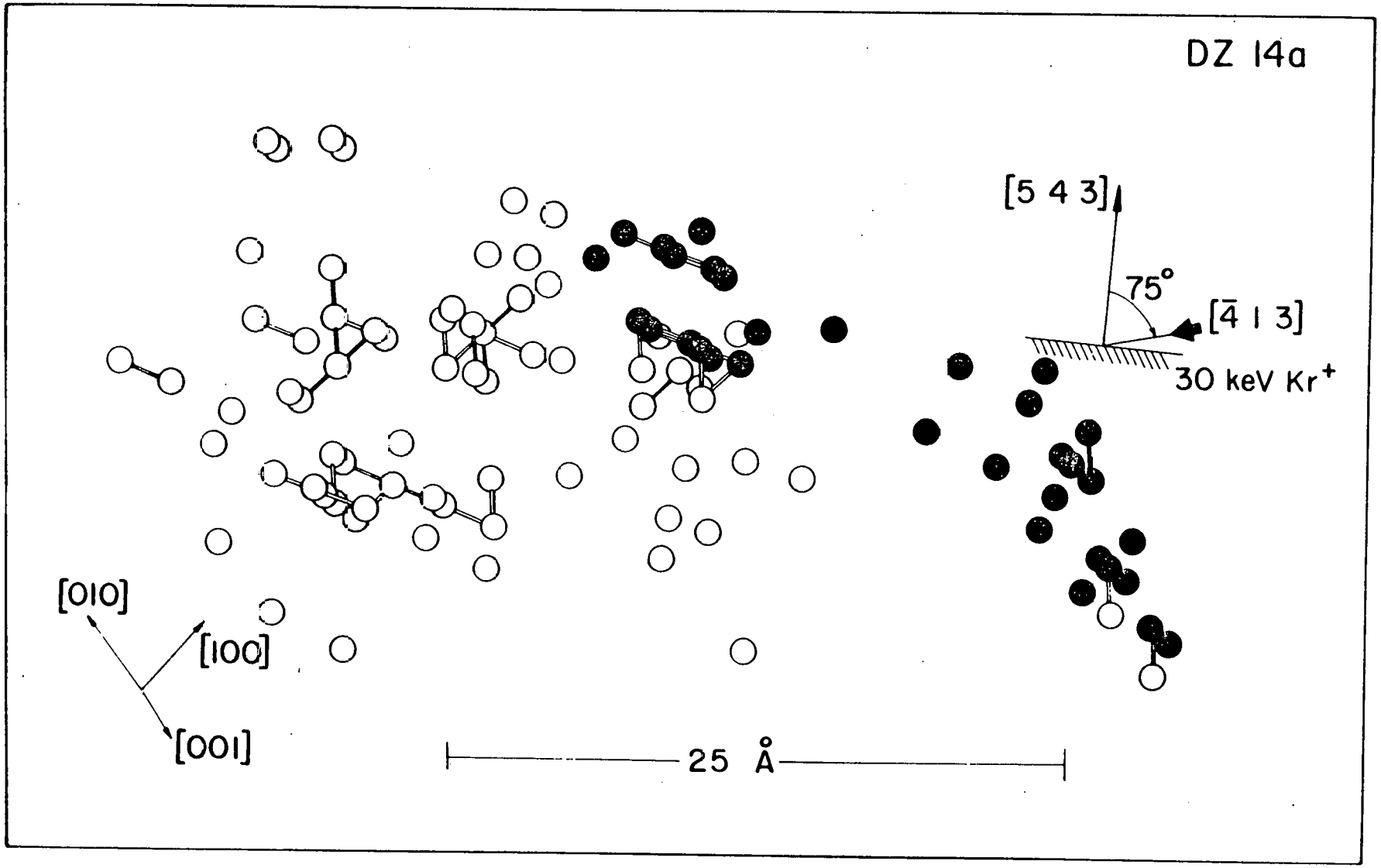

Figure 7 a

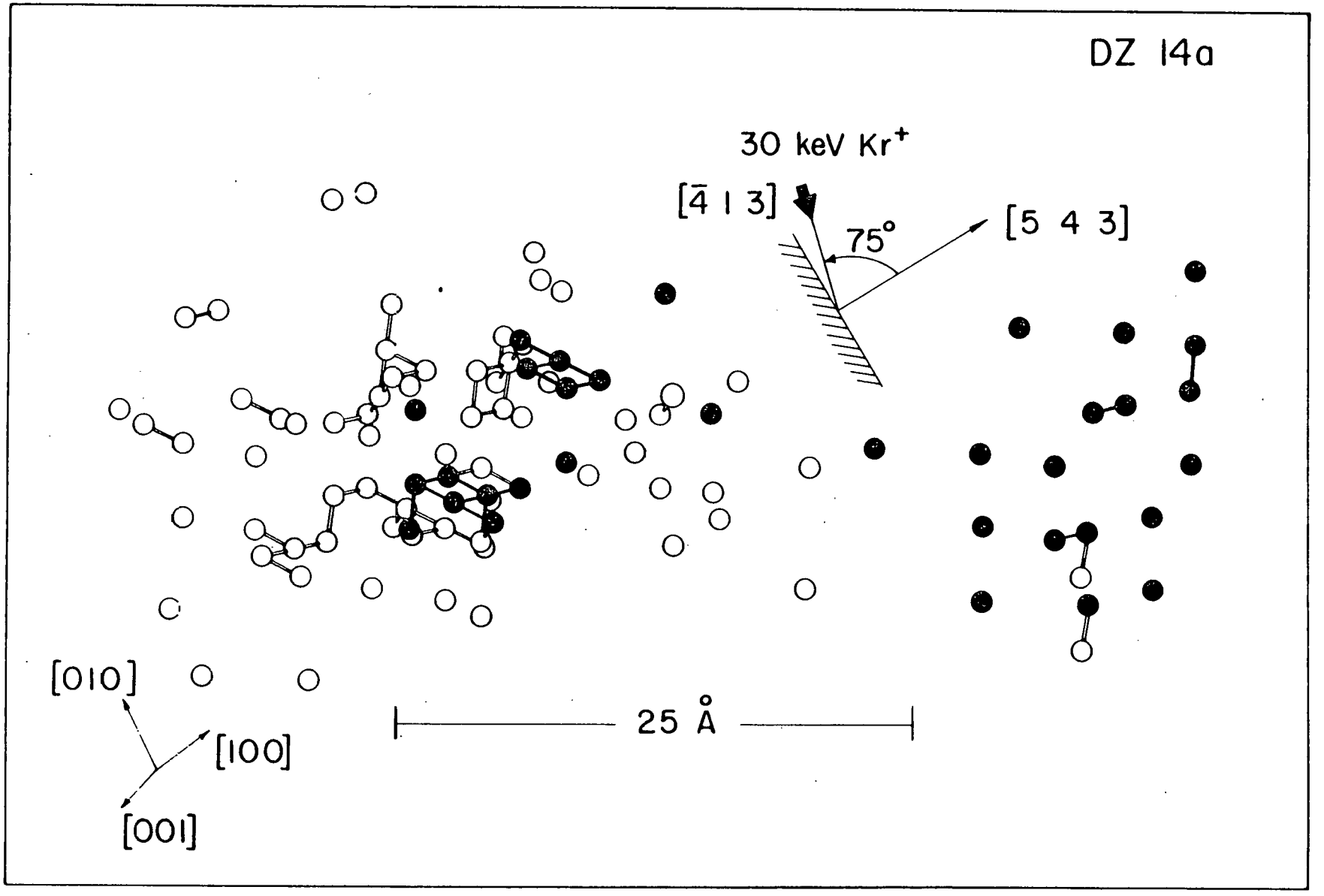

Figure 7 b

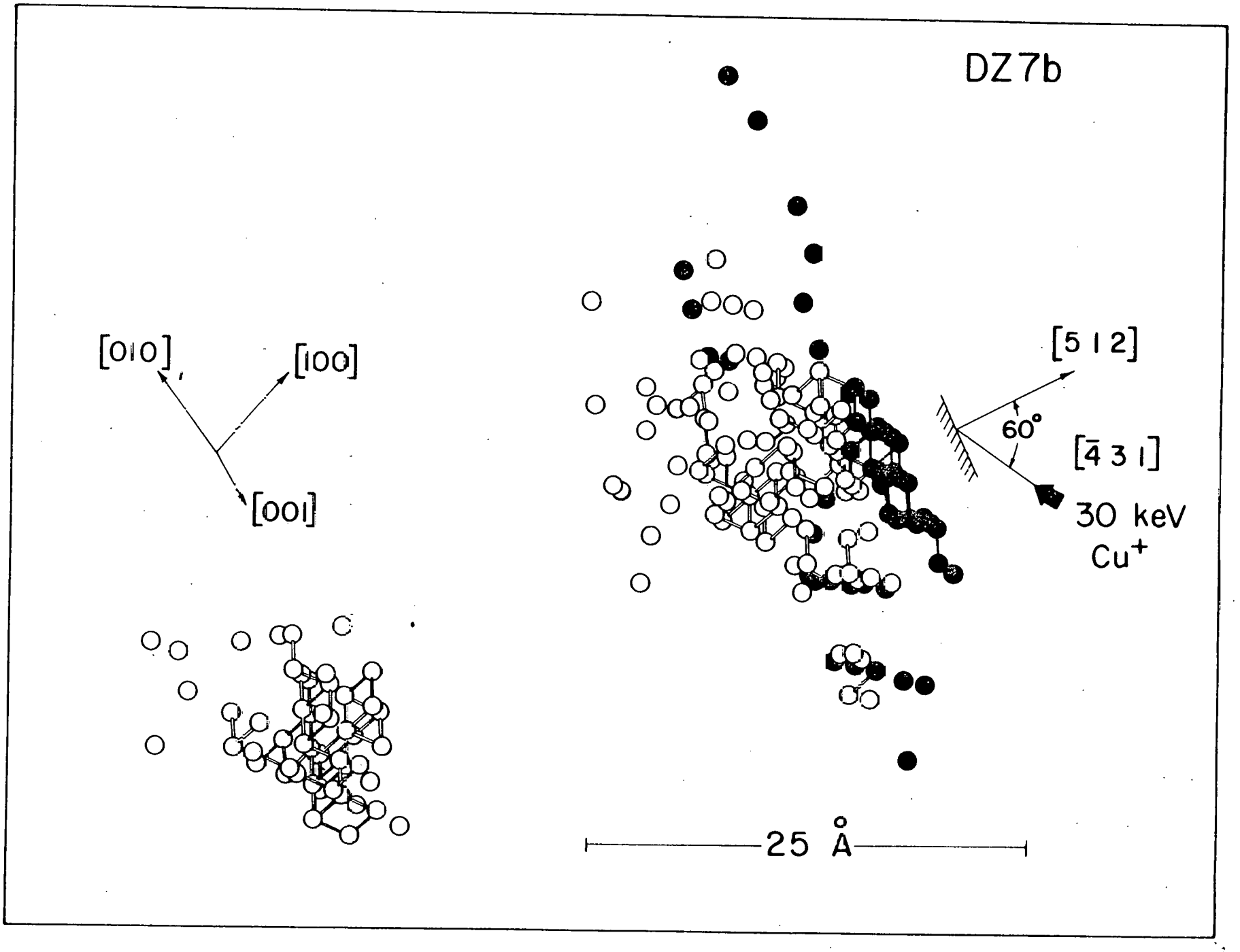

Figure 8 a

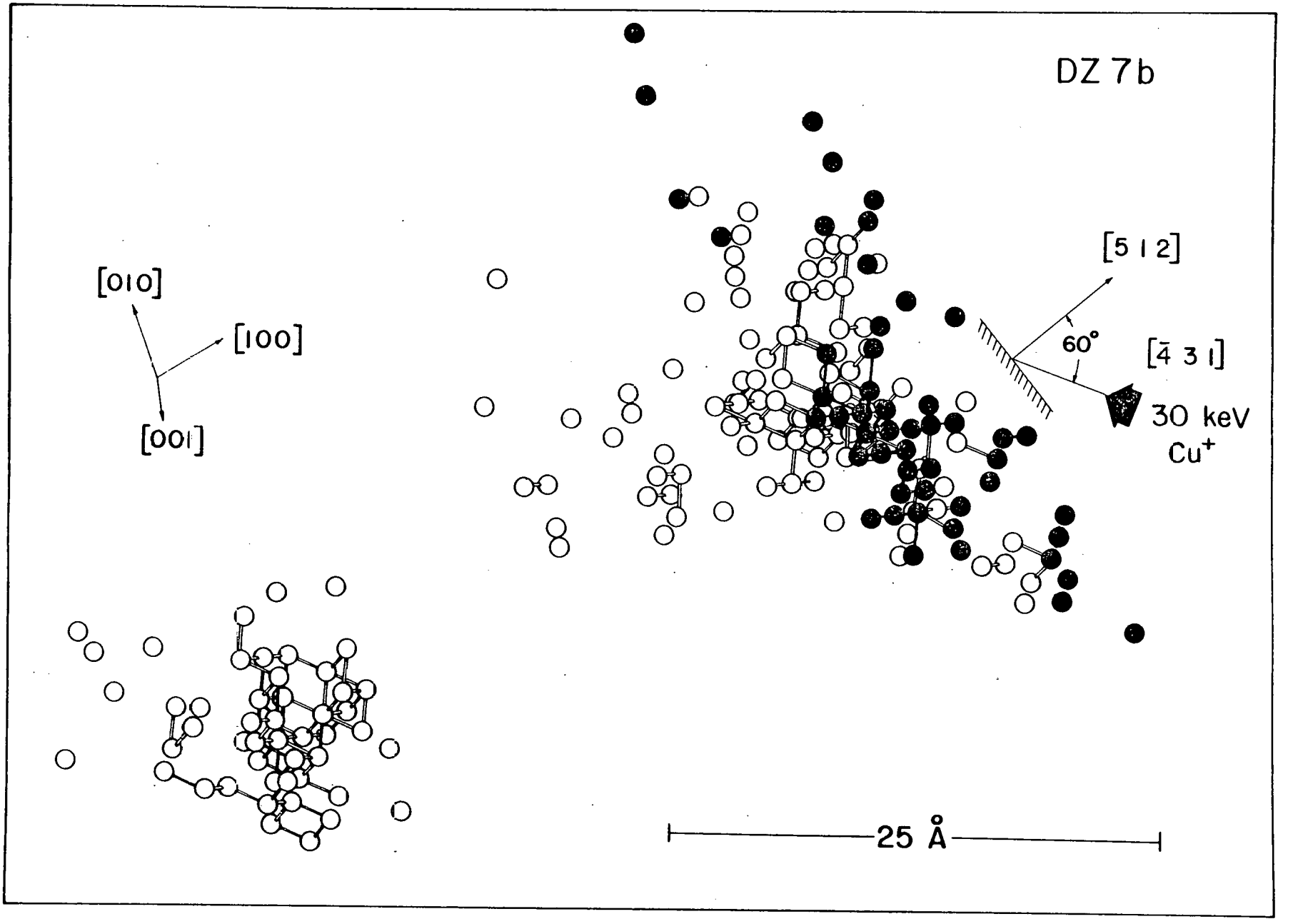

Figure 8 b

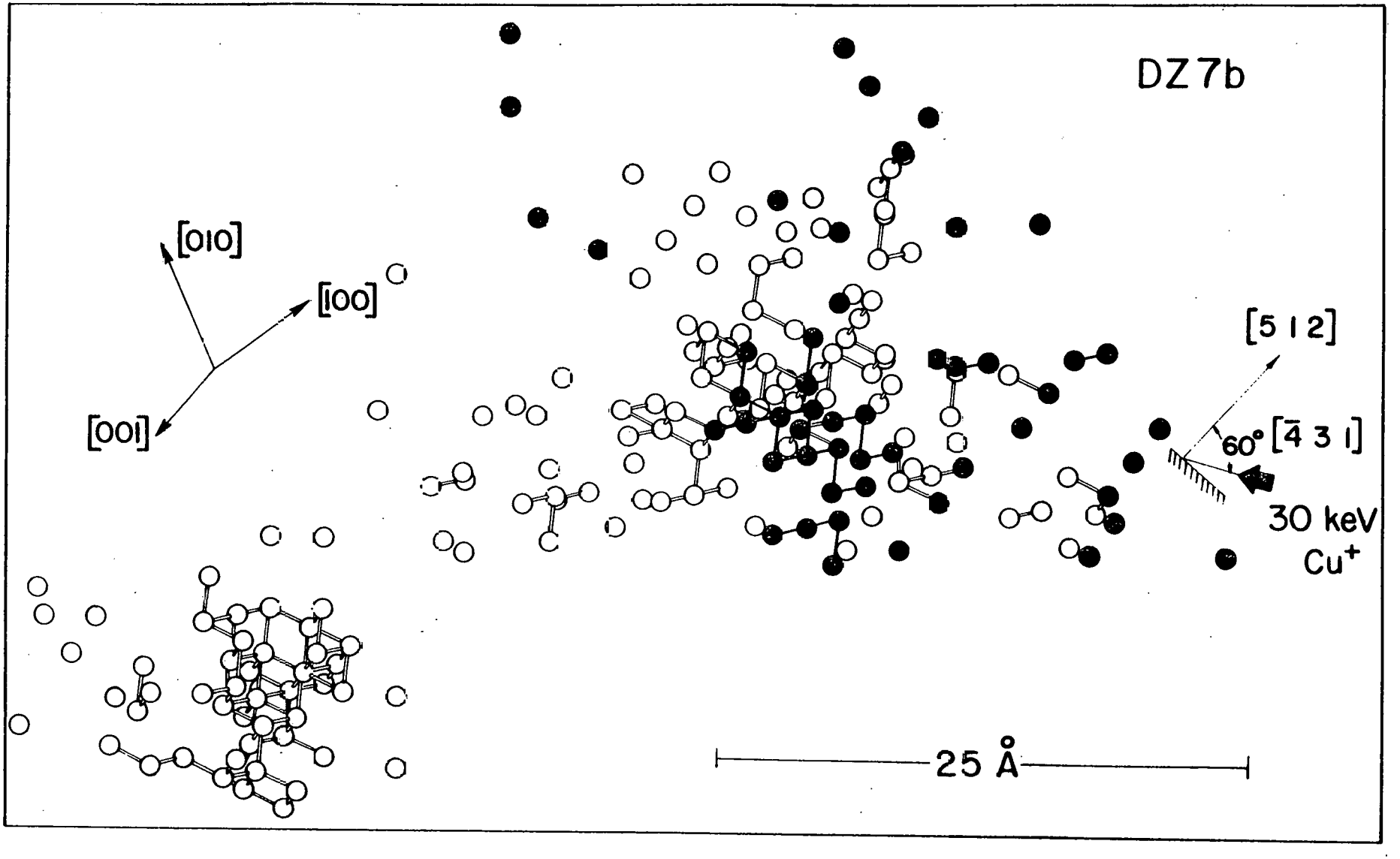

Figure 8 c

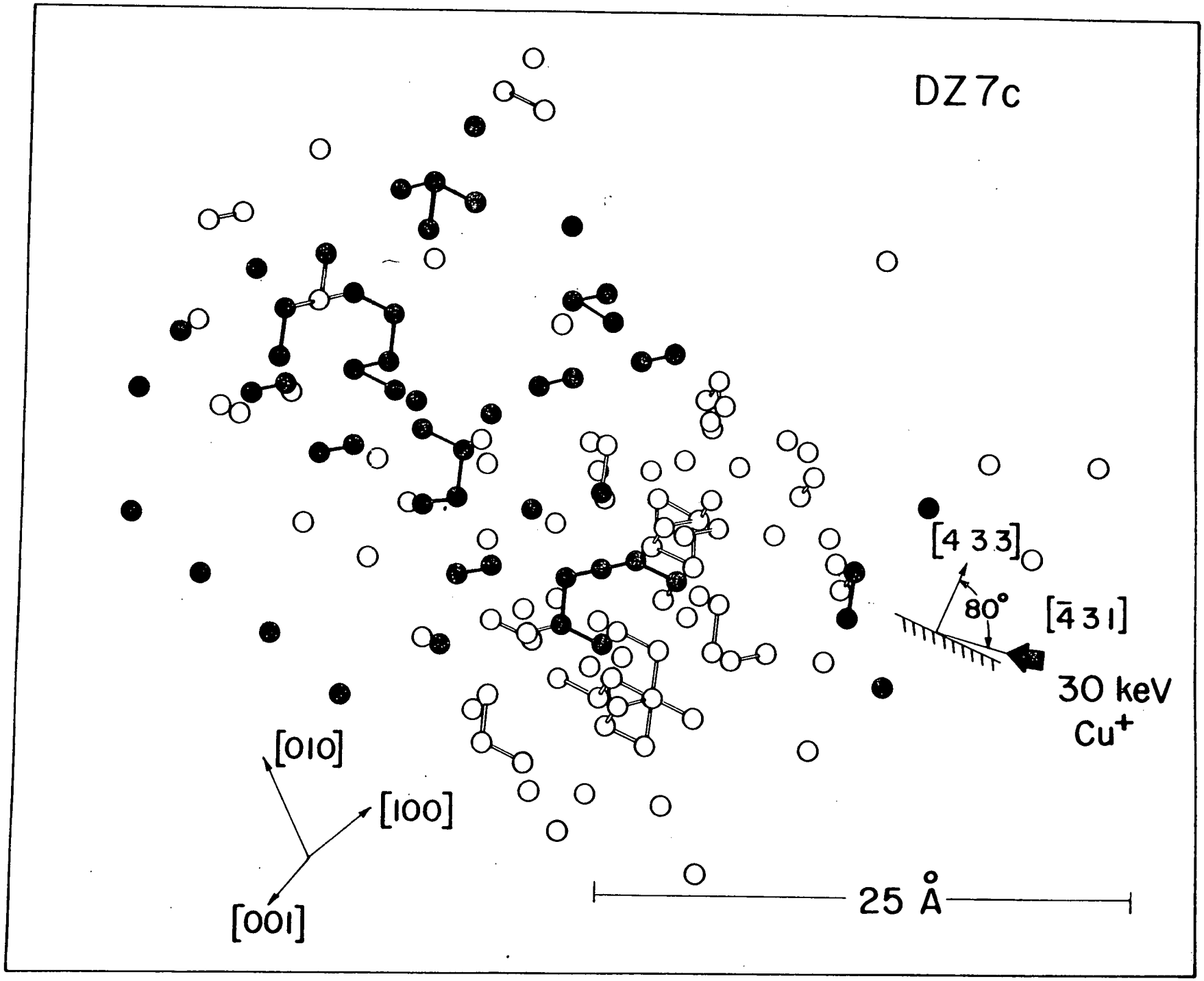

Figure 6

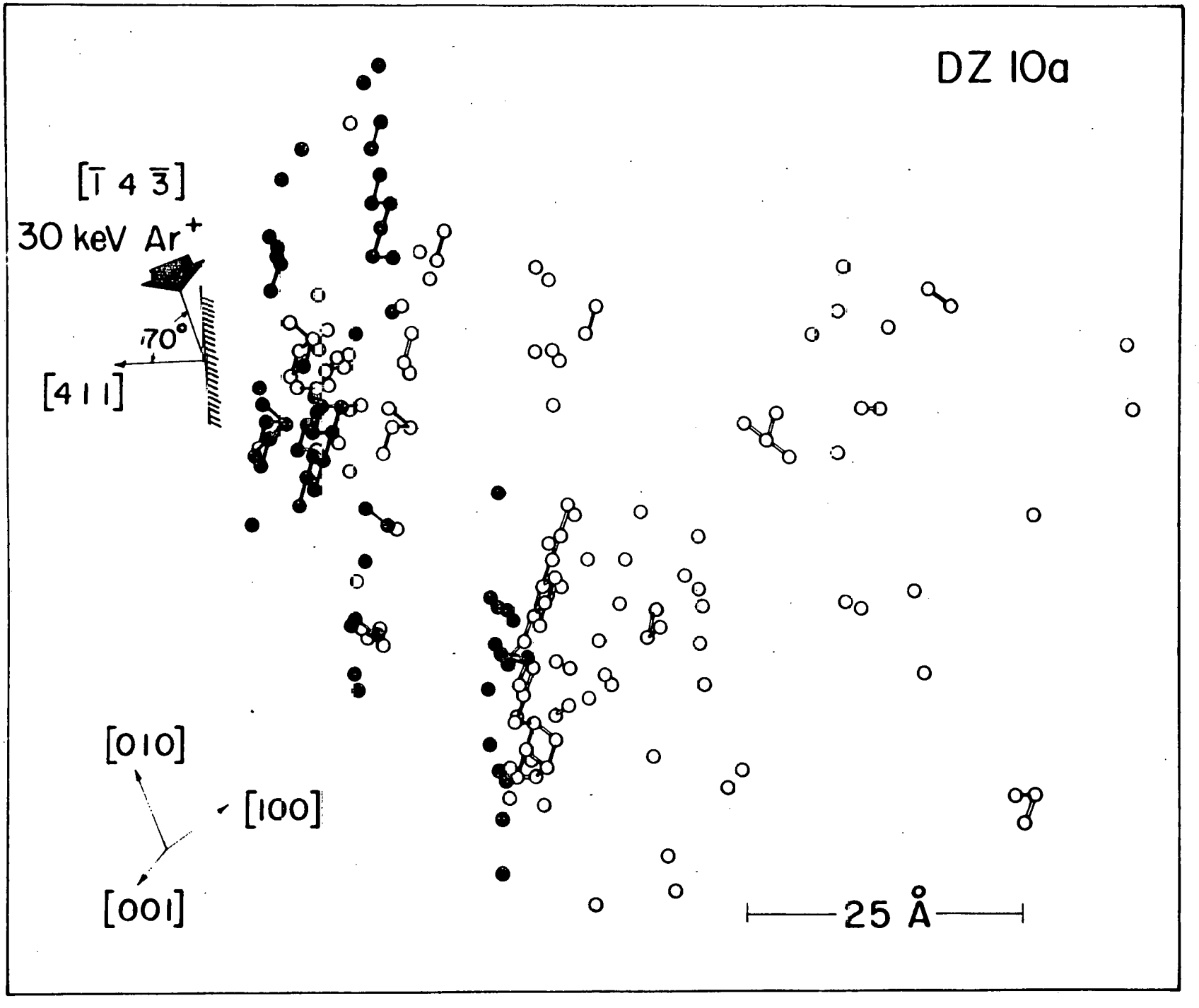

Figure 10

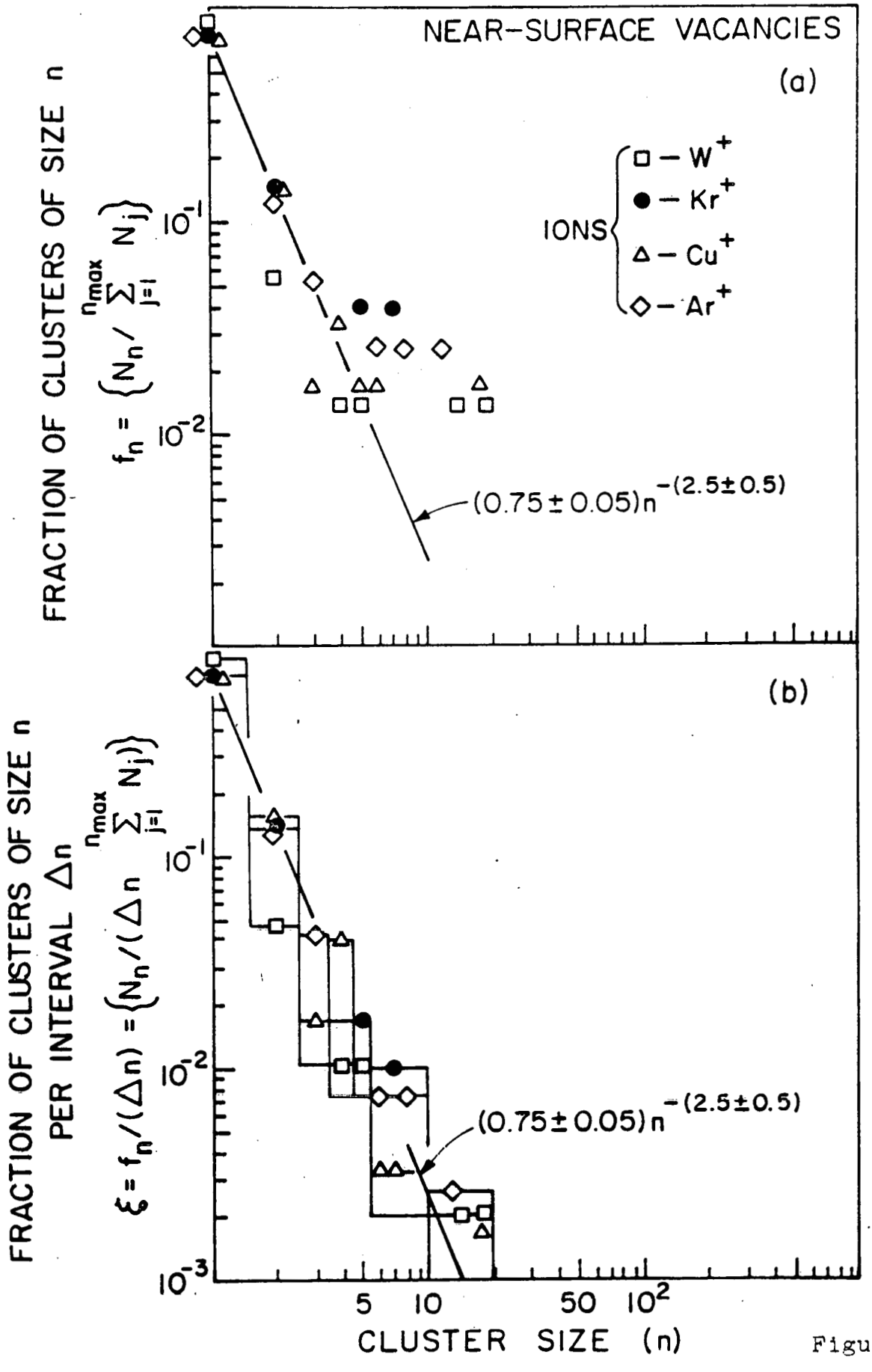
NEAR-SURFACE VACANCIES
(a)
IONS
W+
Kr+
Cu+
Ar+
FRACTION OF CLUSTERS OF SIZE n
$f_n = \{N_n / \sum_{j=1}^{n_{max}} N_j\}$
10^{-1}
10^{-2}
$(0.75 \pm 0.05) n^{-(2.5 \pm 0.5)}$
(b)
FRACTION OF CLUSTERS OF SIZE n PER INTERVAL Δn
$\xi = f_n/(\Delta n) = \{N_n/(\Delta n \sum_{j=1}^{n_{max}} N_j)\}$
10^{-1}
10^{-2}
10^{-3}
$(0.75 \pm 0.05) n^{-(2.5 \pm 0.5)}$
5
10
50
10^2
CLUSTER SIZE (n)

Figure 11

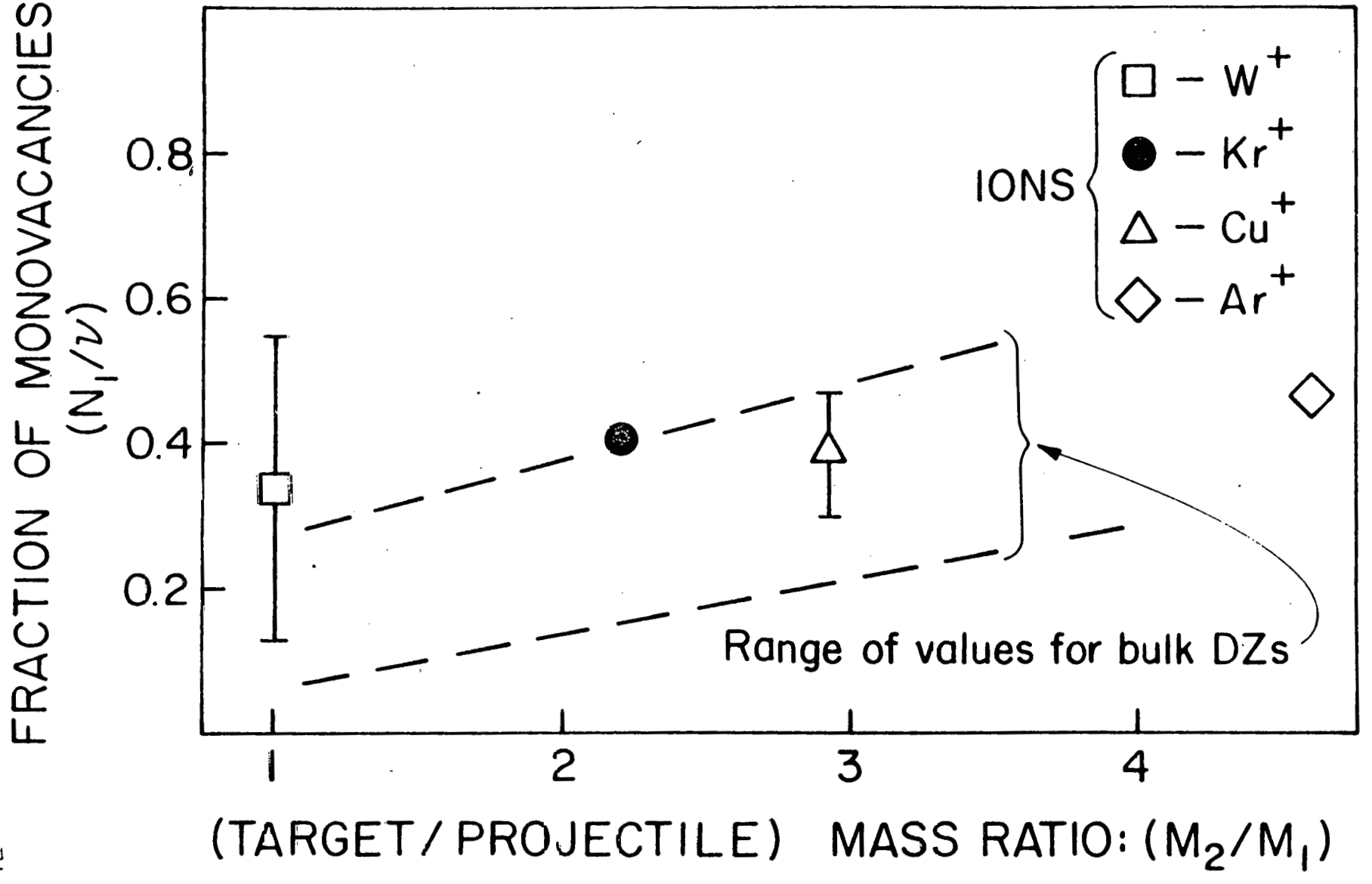
FRACTION OF MONOVACANCIES
(N_1/ν)
0.8
0.6
0.4
0.2
1
2
3
4
(TARGET/PROJECTILE) MASS RATIO: (M_2/M_1)
IONS
□ – W^+
● – Kr^+
△ – Cu^+
◇ – Ar^+
Range of values for bulk DZs

Figure 12

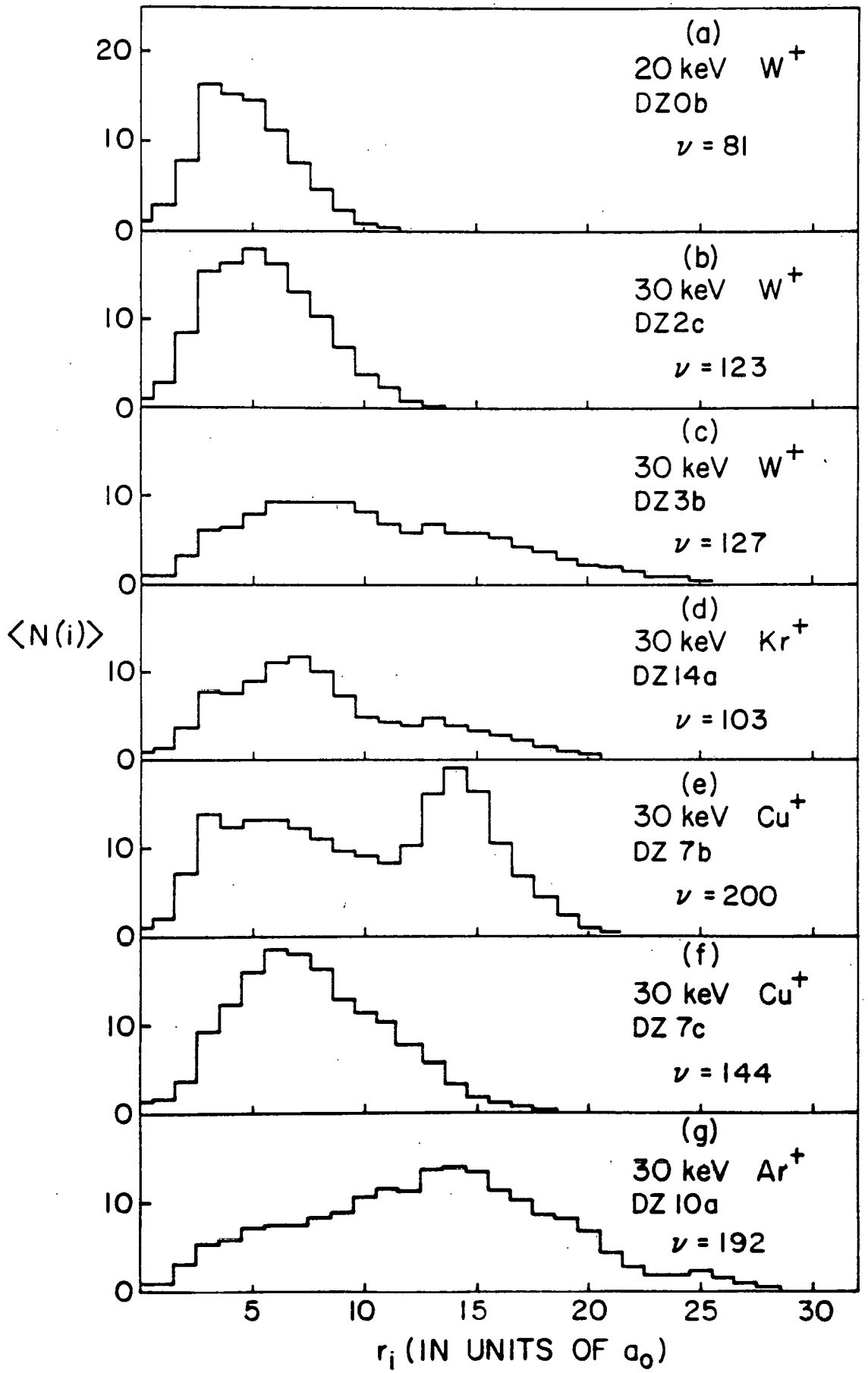
(a)
20 keV W+
DZ0b
ν = 81
(b)
30 keV W+
DZ2c
ν = 123
(c)
30 keV W+
DZ3b
ν = 127
(d)
30 keV Kr+
DZ14a
ν = 103
(e)
30 keV Cu+
DZ 7b
ν = 200
(f)
30 keV Cu+
DZ 7c
ν = 144
(g)
30 keV Ar+
DZ 10a
ν = 192
<N(i)>
0
10
20
5
10
15
20
25
30
ri (IN UNITS OF a0)

Figure 13

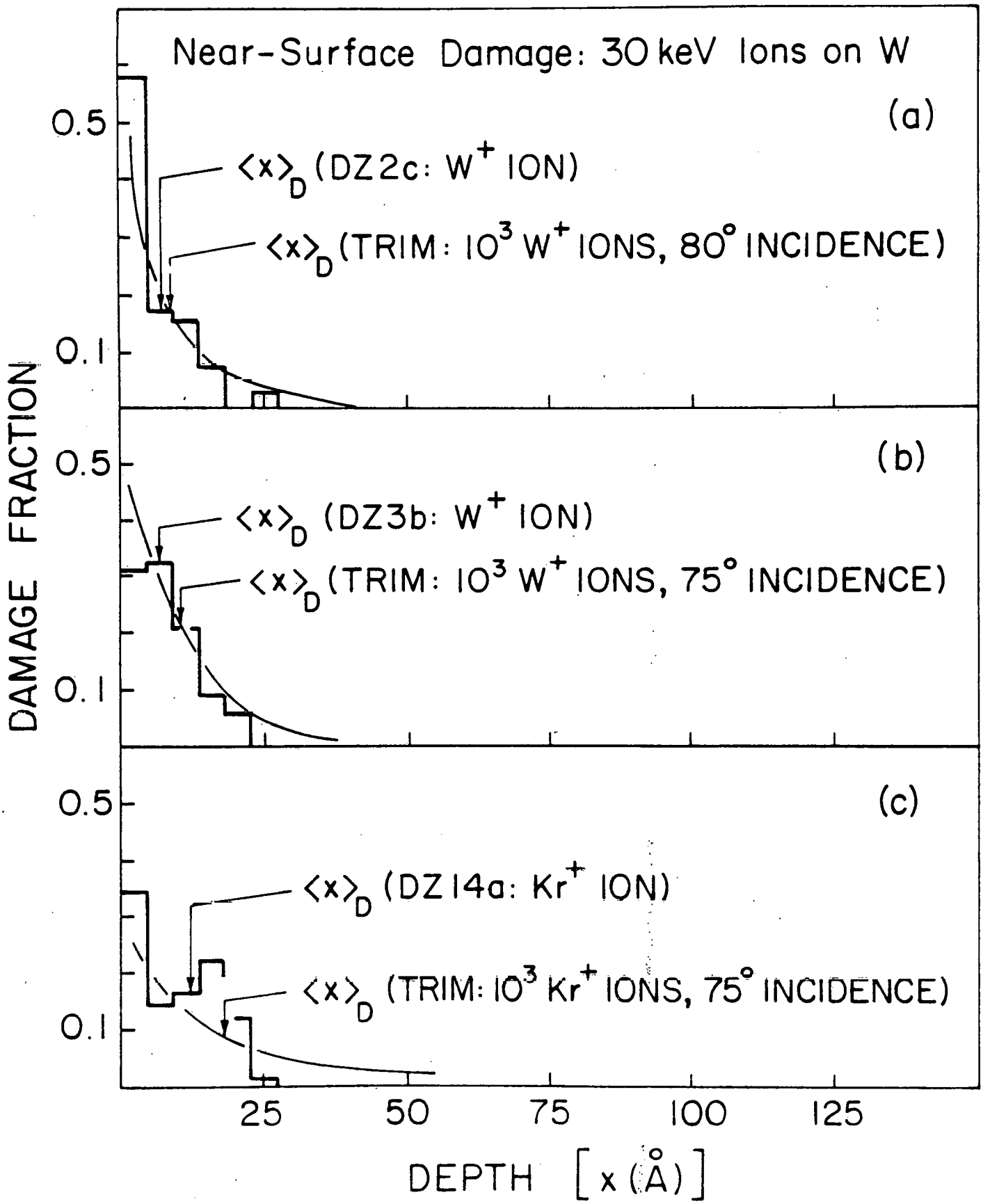
Near-Surface Damage: 30 keV Ions on W
(a)
0.5
0.1
$\langle x \rangle_D$ (DZ2c: W^+ ION)
$\langle x \rangle_D$ (TRIM: 10^3 W^+ IONS, 80° INCIDENCE)
(b)
0.5
0.1
$\langle x \rangle_D$ (DZ3b: W^+ ION)
$\langle x \rangle_D$ (TRIM: 10^3 W^+ IONS, 75° INCIDENCE)
(c)
0.5
0.1
$\langle x \rangle_D$ (DZ14a: Kr^+ ION)
$\langle x \rangle_D$ (TRIM: 10^3 Kr^+ IONS, 75° INCIDENCE)
DAMAGE FRACTION
25
50
75
100
125
DEPTH [x (Å)]

Figure 14 a-c

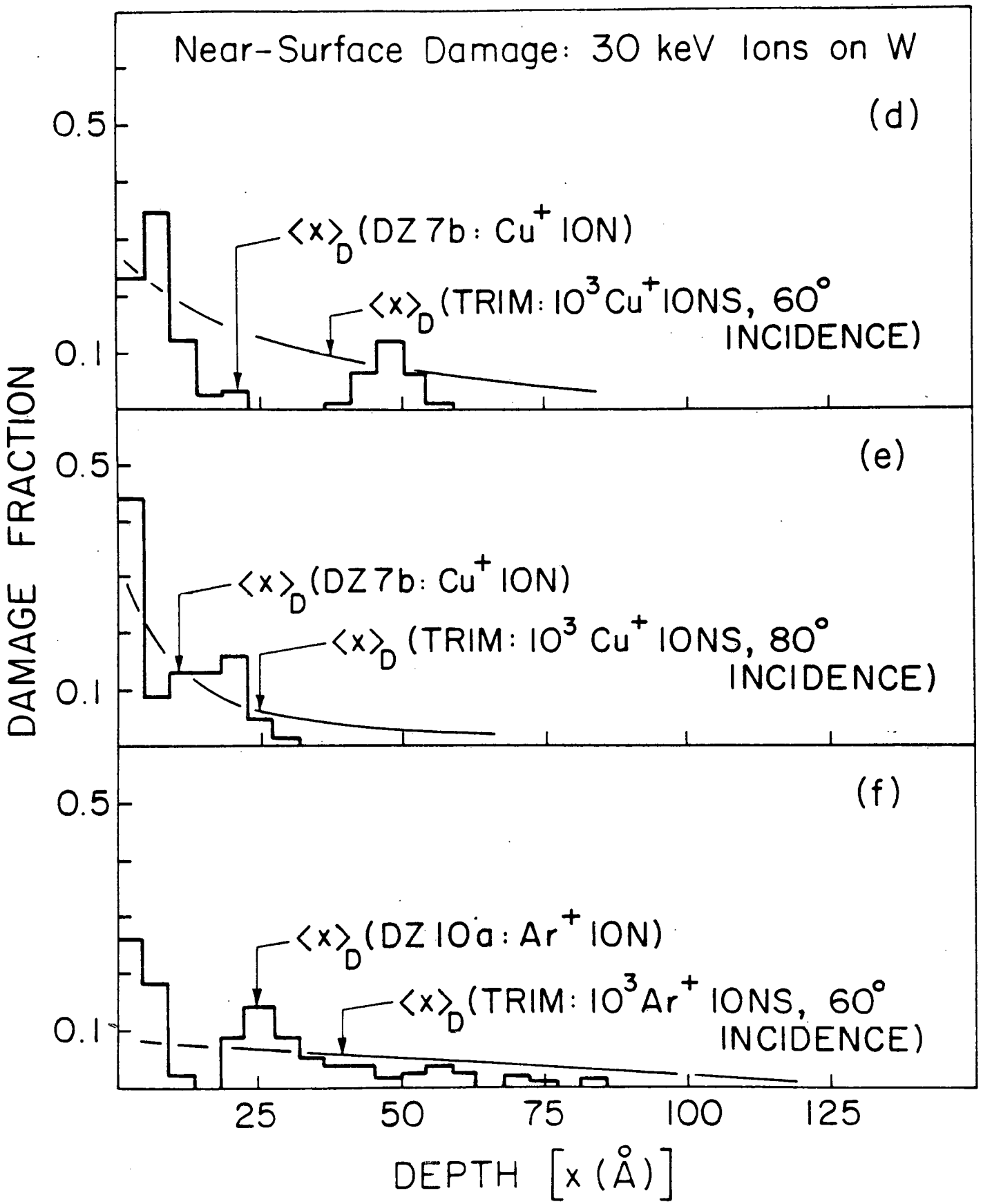
Near-Surface Damage: 30 keV Ions on W
(d)
(e)
(f)
0.5
0.1
DAMAGE FRACTION
⟨x⟩D (DZ 7b: Cu+ ION)
⟨x⟩D (TRIM: 10³ Cu+ IONS, 60° INCIDENCE)
⟨x⟩D (TRIM: 10³ Cu+ IONS, 80° INCIDENCE)
⟨x⟩D (DZ 10a: Ar+ ION)
⟨x⟩D (TRIM: 10³ Ar+ IONS, 60° INCIDENCE)
25
50
75
100
125
DEPTH [x (Å)]

Figure 14 d-f

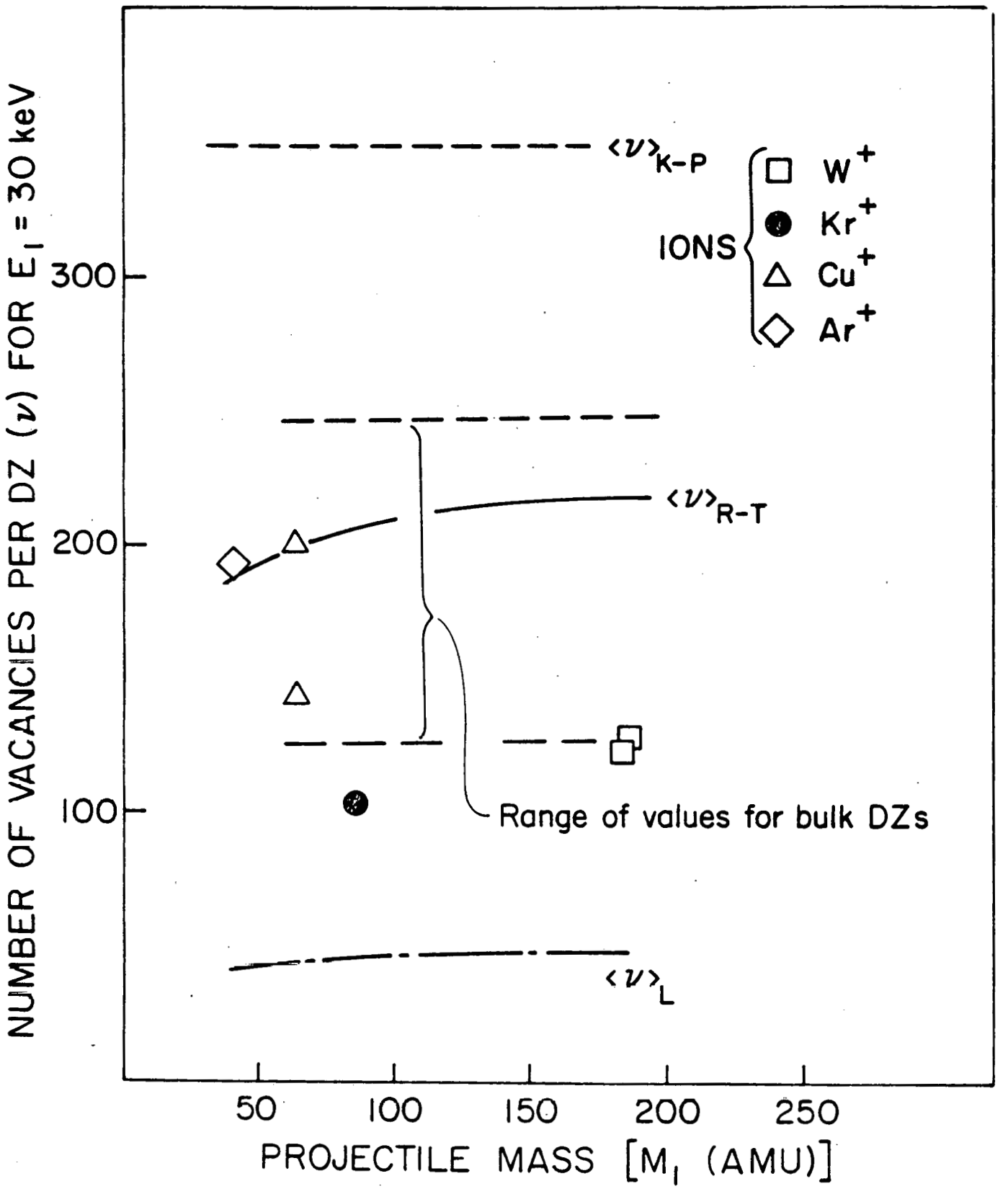
NUMBER OF VACANCIES PER DZ (ν) FOR E1 = 30 keV
300
200
100
50
100
150
200
250
PROJECTILE MASS [M1 (AMU)]
⟨ν⟩K-P
⟨ν⟩R-T
⟨ν⟩L
IONS
W+
Kr+
Cu+
Ar+
Range of values for bulk DZs

Figure 15

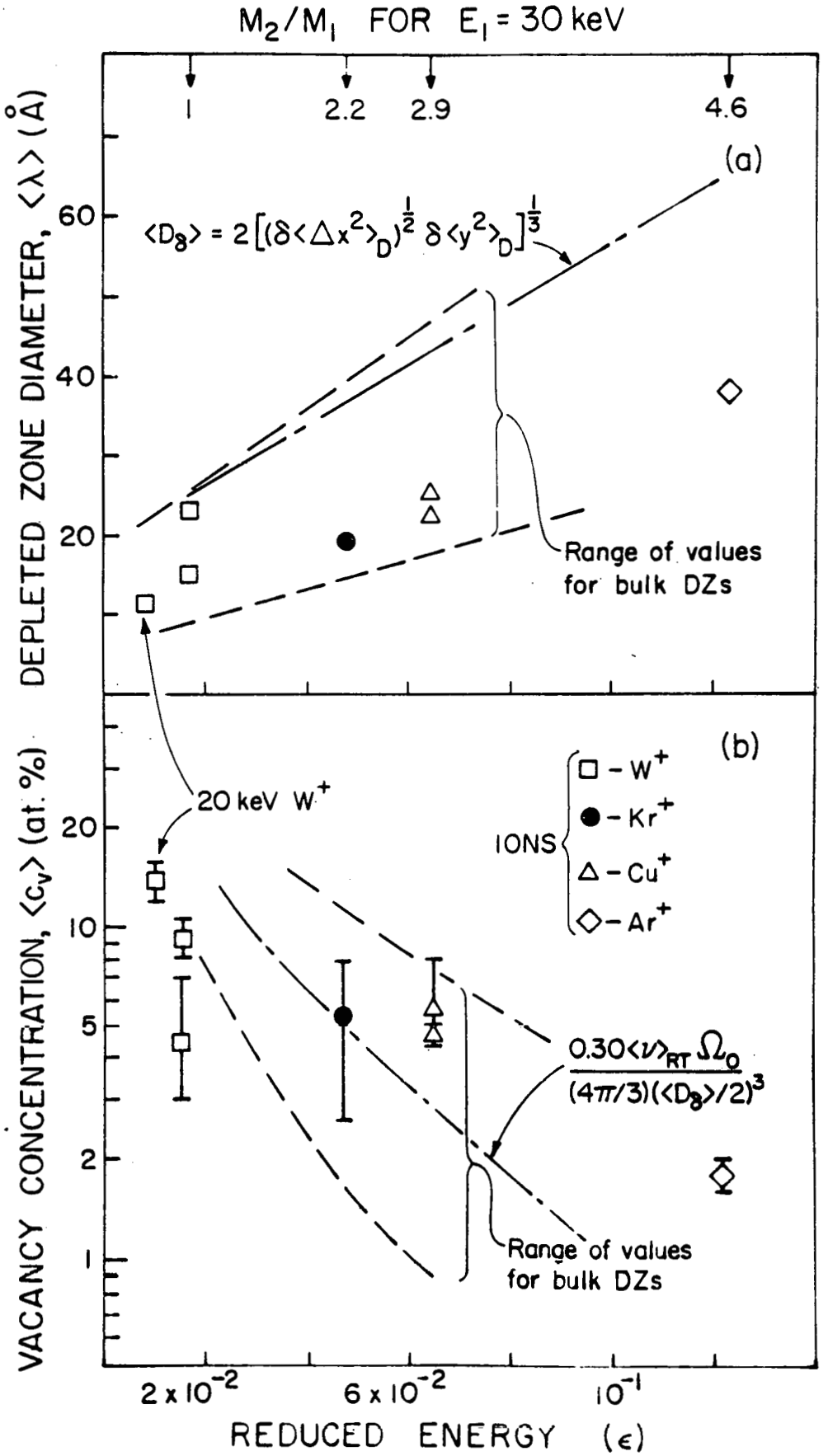
M_2/M_1 FOR E_1 = 30 keV
1
2.2
2.9
4.6
(a)
$\langle D_\delta \rangle = 2[(\delta\langle\Delta x^2\rangle_D)^{\frac{1}{2}}\,\delta\langle y^2\rangle_D]^{\frac{1}{3}}$
Range of values for bulk DZs
DEPLETED ZONE DIAMETER, $\langle\lambda\rangle$ (Å)
60
40
20
(b)
20 keV W^+
IONS
□ - W^+
● - Kr^+
△ - Cu^+
◇ - Ar^+
$\frac{0.30\langle\nu\rangle_{RT}\,\Omega_0}{(4\pi/3)(\langle D_\delta\rangle/2)^3}$
Range of values for bulk DZs
VACANCY CONCENTRATION, $\langle c_v\rangle$ (at. %)
20
10
5
2
1
2×10^{-2}
6×10^{-2}
10^{-1}
REDUCED ENERGY (ϵ)

Figure 16

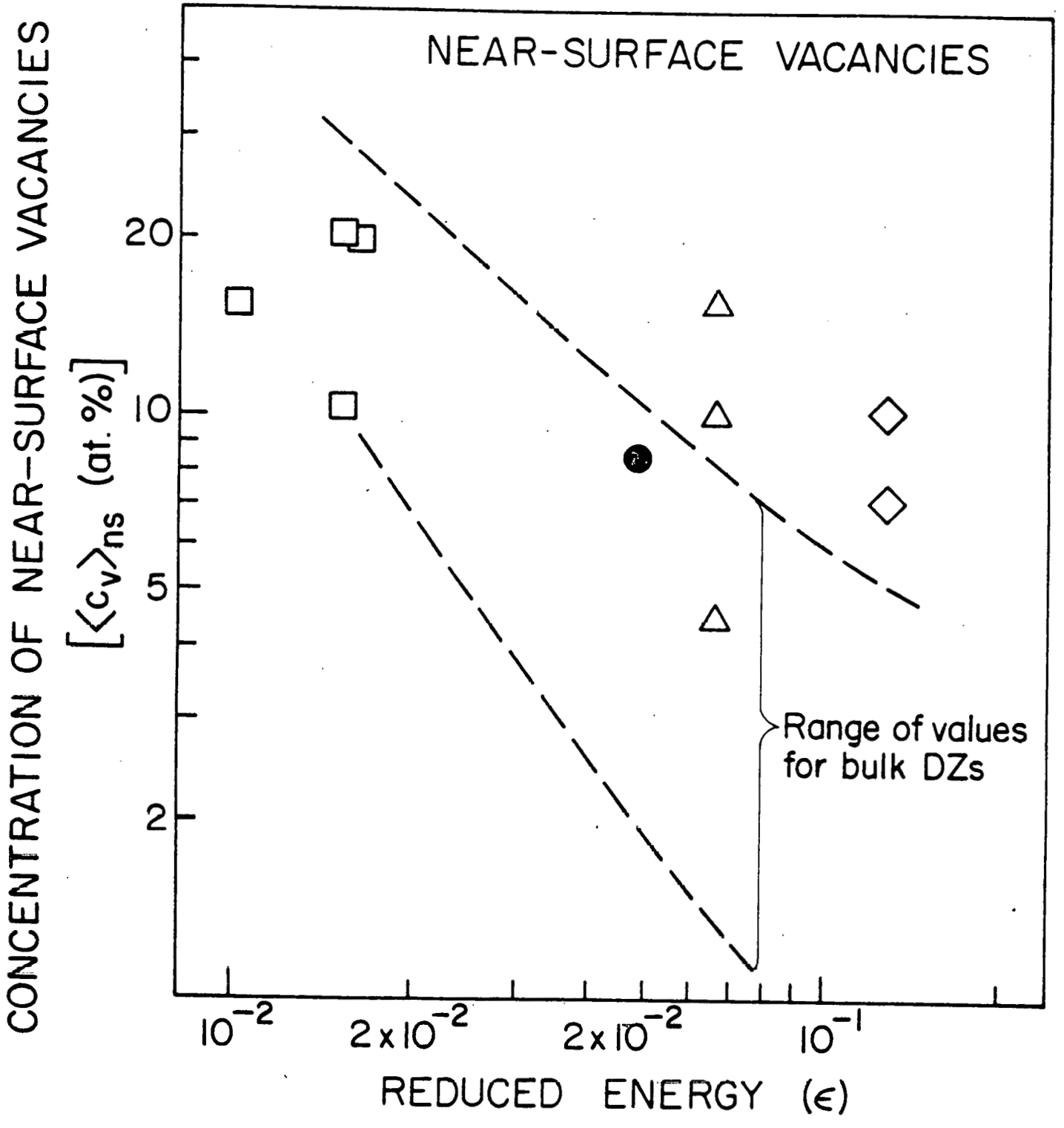
NEAR-SURFACE VACANCIES
CONCENTRATION OF NEAR-SURFACE VACANCIES
$[\langle c_v \rangle_{ns}$ (at. %)$]$
20
10
5
2
Range of values
for bulk DZs
10^{-2}
2×10^{-2}
2×10^{-2}
10^{-1}
REDUCED ENERGY (ϵ)

Figure 17

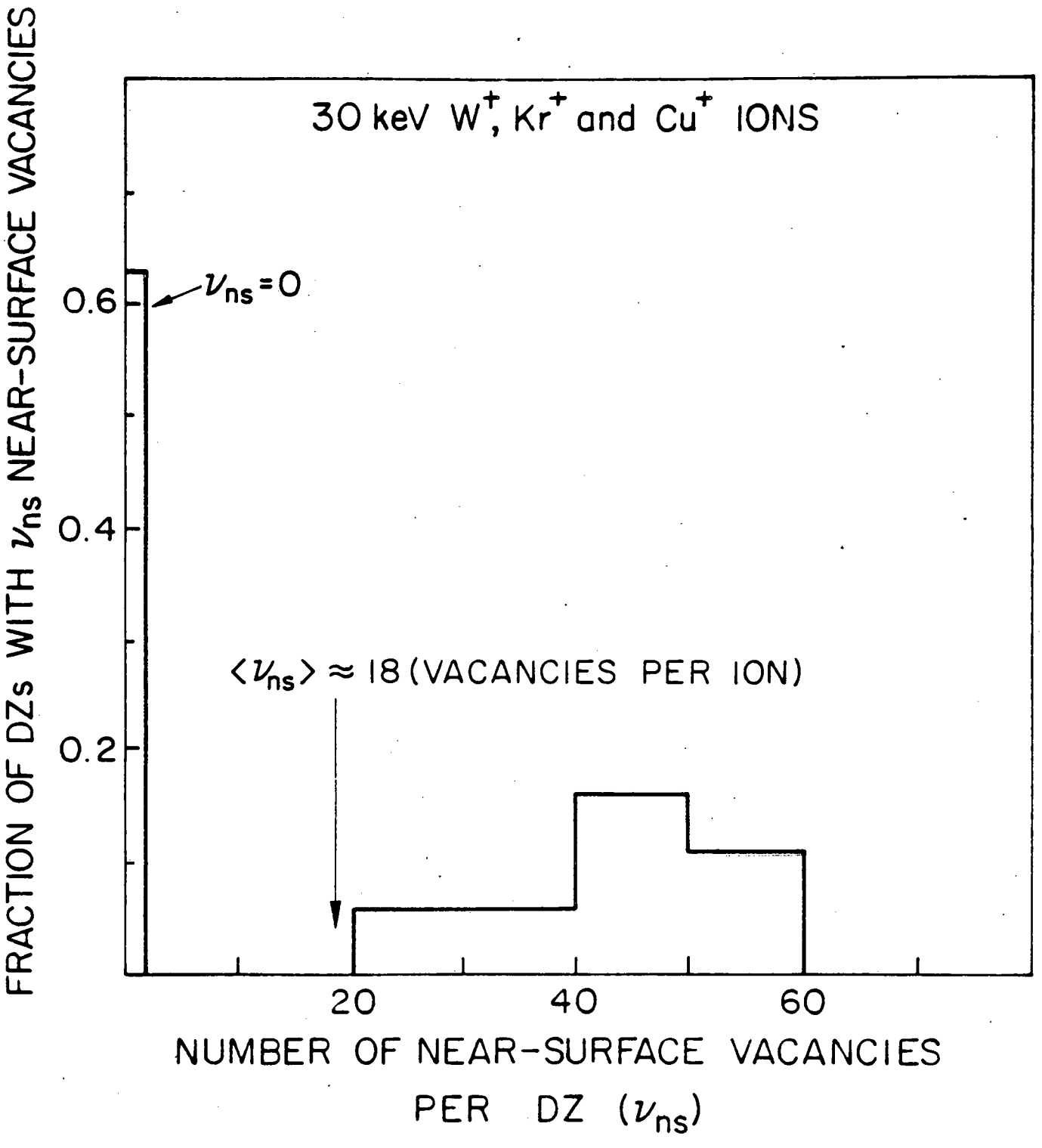
30 keV W+, Kr+ and Cu+ IONS
FRACTION OF DZs WITH νns NEAR-SURFACE VACANCIES
0.6
0.4
0.2
νns = 0
⟨νns⟩ ≈ 18 (VACANCIES PER ION)
20
40
60
NUMBER OF NEAR-SURFACE VACANCIES
PER DZ (νns)

Figure 18

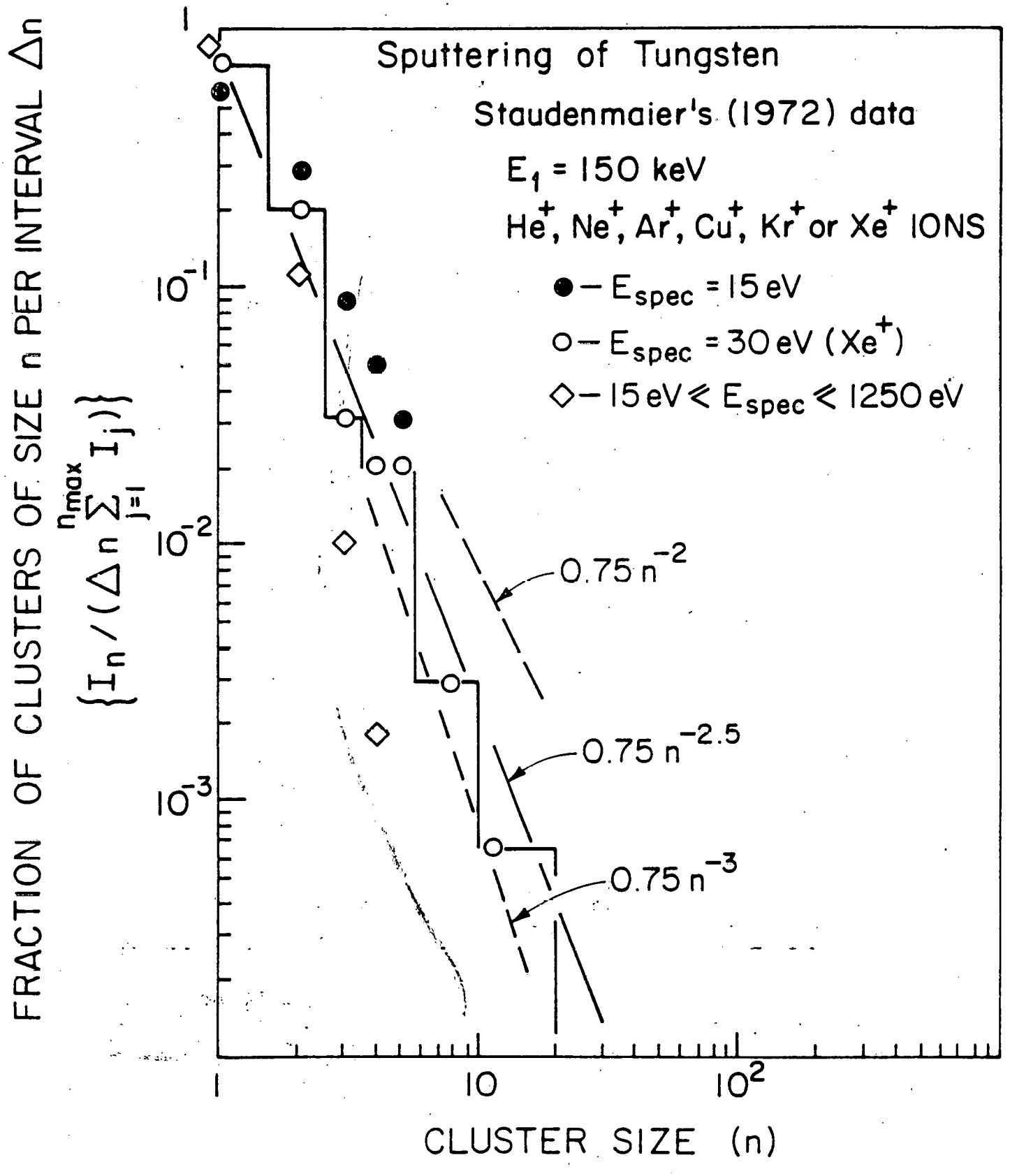
Sputtering of Tungsten
Staudenmaier's (1972) data
E_1 = 150 keV
He^+, Ne^+, Ar^+, Cu^+, Kr^+ or Xe^+ IONS
● – E_{spec} = 15 eV
○ – E_{spec} = 30 eV (Xe^+)
◇ – 15 eV ≤ E_{spec} ≤ 1250 eV
$0.75\,n^{-2}$
$0.75\,n^{-2.5}$
$0.75\,n^{-3}$
FRACTION OF CLUSTERS OF SIZE n PER INTERVAL Δn
$\{I_n / (\Delta n \sum_{j=1}^{n_{max}} I_j)\}$
1
10^{-1}
10^{-2}
10^{-3}
1
10
10^2
CLUSTER SIZE (n)

Figure 19